International Journal of Disaster Risk Reduction 136 (2026) 106053

Contents lists available at ScienceDirect

International Journal of Disaster Risk Reduction

journal homepage: www.elsevier.com/locate/ijdrr

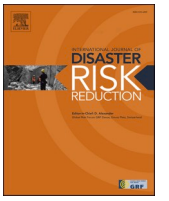

Flood-induced traffic congestion and accessibility loss for urban road networks using agent-based simulation: The case study of Bristol, UK

Ke He [a,*], Neil Carhart [a], Maria Pregnolato [b], Raffaele De Risi [a]

[a] Department of Civil Engineering, University of Bristol, Bristol, BS8 1TR, UK
[b] Department of Civil Engineering, Delft University of Technology, Mekelweg 5, 2628 CD, Delft, Netherlands

A B S T R A C T

This study proposes a methodology for assessing the impact of flood-induced functional disruptions on urban road networks through an agent-based traffic simulation. Network functionality is altered by reducing roads' free-flow speeds using a risk-based approach, and traffic is appraised considering agent-based traffic dynamics. MATSim, an open-source transport simulator, is employed to model dynamic traffic redistribution and congestion under both baseline (non-flood) and flood conditions of the urban road transportation network. The methodology is applied to the city of Bristol, UK, which is chosen for its complex road layout and flood susceptibility. Key indicators, including travel speed ratios, redistribution ratios, changes in agent count, and time-based isochrones, are used to assess variations in congestion and accessibility under both baseline and flood conditions. This study further advances existing approaches by comparing the spatial shifts of congestion hotspots before and after flooding, and by integrating hazard scenarios to predict potential future congestion patterns and their subsequent impacts on the accessibility of critical facilities, such as the Bristol Royal Infirmary. Results indicate a substantial redistribution of traffic from flood-affected minor roads to central arterial routes, leading to increased congestion and reduced accessibility, which can be particularly detrimental to emergency services that require rapid access to affected areas. The findings highlight the importance of simulating agent-level behavioural responses to network disruption caused by flooding and provide a transferable framework for assessing urban transport resilience during flood events.

1. Introduction

With the advancement of urbanisation, the impact of natural hazards has increased. Among hazards, floods have a particularly significant impact on urban areas [1]. In urban areas, roads are among the most visibly affected infrastructure elements by flooding. The effect of floods on roads can be categorised into two broad typologies: structural damage and functional disruption [2]. Structural damage to roads caused by flooding typically manifests as cracks, collapses, and erosion, and generally occurs only during extreme flood events [3–5]. In contrast, functional disruption of the road network is characterised by increased travel times, longer detour distances, or complete vehicular inaccessibility ([2,6,7]; [8]. Unlike structural damage, functional interruption can occur during any flood event. Consequently, research on the functional disruption of road networks due to flooding has become an increasingly important topic.

The most common approach to assessing functional disruption of road networks is the integration of road network data with flood hazard maps to analyse the inundation depth for each road [1,9–14]. The inundation depth and the corresponding return period indicate the level of flood hazard to which each road is exposed. However, additional metrics are required to quantify traffic disruption. As roads primarily serve vehicles, assessing their vulnerability to flooding is key to determining the road network's

* Corresponding author.
E-mail address: ke.he@bristol.ac.uk (K. He).

https://doi.org/10.1016/j.ijdrr.2026.106053
Received 1 September 2025; Received in revised form 19 January 2026; Accepted 8 February 2026
Available online 10 February 2026

usability. When vehicles are unable to transit a flooded road, this indicates a loss of network functionality [7,15,16]. Thus, integrating the road network (exposure), vehicle stability (vulnerability), and flood frequency and intensity (hazard) forms the basis for assessing the risk of functional loss in road networks during flooding [17,18].

Open-source road network data (e.g., OpenStreetMap) can provide the exposure/topology needed for graph-based analysis in which intersections are nodes and roads/bridges are links ([19–24]; [25]; [26–29]; [30]; [14,16]). Vulnerability can be characterised via vehicle stability experiments and depth–velocity effects, with continuous depth–speed relations translating hazard to link performance decrements ([31–33]; [2,34–37]). Flood hazard is obtained from hydrodynamic models (e.g., LISFLOOD-FP, HEC-RAS) that produce depth/velocity fields [38–41]. The road accessibility can be screened deterministically (e.g., comparing flood resistance capacity of the vehicle and exact flood), while probabilistic risk methods employ fragility curves to estimate functional loss; we follow this latter approach by mapping hazard–vulnerability interactions to a probability of network functional loss and reducing link performance parameters accordingly [7,15,17,18,42,43].

Building on previous work that developed deterministic and probabilistic flood-related road functionality models for emergency vehicles in Bristol [16,43], this paper treats the resulting link-level functionality risk maps as given inputs. Here, risk-informed speed reductions are embedded in an agent-based MATSim simulation, with travel demand synthesised from land-use and census data to generate realistic OD flows. This enables a dynamic assessment of congestion redistribution, bottlenecks and isochrone-based emergency accessibility under flood-impaired network conditions. Specifically, we map the functional-loss probability into the percentage of a road link's functional impairment under flooding. Furthermore, we couple link-level functional loss with an agent-based traffic simulation to capture the resulting dynamic network response and its subsequent impact on accessibility to critical facilities. City centres bisected by a river and served by a few bridges (such as Bristol) are particularly susceptible to functional disruption and congestion migration, which can impair network accessibility from critical facilities. In dynamic settings, network functionality loss triggers a cascade of congestion that alters accessibility. These gaps in behaviourally realistic, time-resolved analyses motivate our integrated framework and its application to Bristol to quantify pre-/post-flood shifts in congestion and hospital accessibility under disruption.

The remainder of the paper is organised as follows. Section 2 summarises the literature about agent-based traffic simulations. Section 3 details the methodology for assessing traffic congestion, vehicle redistribution, potential bottlenecks, and road network accessibility. Section 4 introduces the Bristol case study in the West of England, where the city-centre network is susceptible to fluvial flooding due to its proximity to the river. Also, it demonstrates the proposed framework to analyse congestion, redistribution, and accessibility outcomes. Section 5 discusses key findings and the existing limitations of this study and based on these limitations, outlines future research directions and policy applications. Section 6 concludes this study.

2. Literature review

In an agent-based approach, each individual (e.g., vehicles or pedestrians) is represented as an agent whose travel behaviour is simulated, producing a dynamic, bottom-up representation of network-wide traffic flow [44]. When the road network's functionality is compromised, vehicle travel is affected, leading to detours and longer travel times. The most evident consequence is traffic congestion, making traffic simulation and congestion analysis essential for informing mitigation strategies.

The most used platforms for traffic simulation are PTV Visum, PTV VISSIM, SUMO, and MATSim, among others [45,46]. PTV VISSUM is a microscopic simulation tool that models individual vehicles and pedestrians to analyse traffic dynamics, while PTV Visum is a macroscopic modelling platform focused on strategic traffic-flow and demand analysis rather than individual vehicle behaviour [47]. SUMO is an open-source, microscopic traffic simulator that enables detailed modelling and analysis of urban transport networks [48]. MATSim is an agent-based, mesoscopic transport simulator in which individual travellers execute daily plans via a computationally efficient queue-based network model, enabling city- and region-scale applications. Its iterative replanning supports large-scale dynamic network loading with responsive rerouting and day-to-day adaptation, making it well-suited to analyse disruption and congestion redistribution [49,50]. A percolation–contagion formulation has been documented for modelling the spatio-temporal spread and recession of inundation on road graphs via SEIR-style dynamics, yielding time-varying fractions of affected links and allowing validation against observed event footprints [51,52]. Building upon these foundations of hazard evolution, our study extends this logic by introducing a general vulnerability-to-performance translation to evaluate traffic operational impacts.

MATSim has been used to simulate operational urban road networks at city–region scale, with recent work improving runtimes and demonstrating open, multi-modal city models [53,54]. For congestion analysis, MATSim outputs have been used to map spatio-temporal congestion levels and identify hotspot corridors under policy and technology scenarios such as congestion charging and automated-taxi operations [55,56]. For route evaluation, studies draw on MATSim's plan scoring and link-based assignments to examine travellers' route choices and the relative performance of candidate paths under different pricing and cost structures, including integrated land-use–transport contexts [57,58]. Collectively, this body of work establishes MATSim as a mature tool for simulating networks, diagnosing congestion hotspots, and evaluating route-choice behaviour at realistic urban scales.

In MATSim-based traffic modelling, vehicle trajectory data play a crucial role by providing empirical inputs for initialising, calibrating, and validating agent plans. High-frequency GPS probe (“floating-car”) data from on-board devices or smartphones can directly capture per-vehicle paths and speeds with sufficient fidelity for network modelling and diagnostics, as demonstrated by field experiments and large-scale analyses [59–61]. In addition, anonymised mobile-phone data could allow the reconstruction of travellers’ trip chains and trajectories, offering high-coverage observations of traffic flows across the network [62–64]. Although GPS-based and mobile-phone-based trajectory data offer high-fidelity observations of traffic dynamics, their use is constrained by cost, data access, and privacy concerns. This study, therefore, estimates zone-to-zone OD flows from census and land-use data using a constrained

gravity model as a pragmatic alternative [65]. Moreover, complementary multi-scale, data-driven validation has quantified flash-flood travel-time impacts from neighbourhood to city scales using observed traffic conditions but does not simulate agent-level rerouting within a degraded network.

3. Methodology

The methodological workflow of this study comprises three main stages: (1) data collection, (2) traffic simulation, and (3) traffic appraisal. Fig. 1 presents this workflow, which follows the full causal chain of disruption: flood hazard leads to link-level functional loss, which triggers agent rerouting, resulting in network-wide congestion, and ultimately measured as a loss of accessibility.

3.1. Data and case study

The dataset comprises three components: road network topology (Section 3.2), flood hazard and risk (Section 3.3), and OD matrix and agent plan (Section 3.4).

This study provides a consolidated inventory of all input datasets, including source, spatial resolution/CRS, preprocessing steps, and corresponding references (Table 1). This summary ensures reproducibility across the three data pillars used in this study (road network topology, flood hazard/risk and the translation to link attributes, and agents' plans and OD matrices), linking each dataset to its role in the modelling workflow.

The selected case study area is the city of Bristol, United Kingdom (Fig. 2). Bristol is a city located in Southwest England (Fig. 2(a)), positioned along the River Avon, which flows directly through the city centre. This water body contributes to making Bristol a flood-prone area. Additionally, the road network in Bristol city centre (Fig. 2(b)) is highly complex, and the area exhibits significant variations in elevation. Bristol's topography slopes from north to south, and the river bisects the city centre; with only a few cross-river bridges, the road network's connectivity is highly susceptible to flood-induced disruption. These characteristics make Bristol a suitable case study for investigating traffic congestion before and after flood-induced disruptions to the road network.

This study focuses on the transport efficiency of the road network in supporting emergency response vehicles within central Bristol. Thus, the zone containing Bristol Royal Infirmary (BRI) forms the principal case study area, and the transportation network in that area is studied in more detail (Fig. 2(c)).

Central Bristol was selected for three reasons: (i) riverine flood susceptibility along the River Avon, (ii) a complex road topology with limited cross-river redundancy, and (iii) the presence of a major critical facility (Bristol Royal Infirmary). This choice directly supports our objectives of analysing flood-induced congestion redistribution and assessing emergency accessibility.

3.2. Road network topology

The first dataset is the road network, which primarily captures the spatial topology of roads, such as connectivity. Additionally, it features functional attributes that impact traffic performance, including road capacity and free-flow speed. In MATSim, the network topology must include both *nodes* and *links*. Nodes represent intersections and road endpoints, while links denote road segments, bridges, and similar infrastructure elements. Nodes are defined by a unique ID and their geographical coordinates. Links are characterised by a unique ID, the IDs of the two connected nodes, and various attributes such as capacity, free speed, and length. OpenStreetMap is used to extract the road network topology, which is then converted into the required MATSim format for simulation.

The elevation of Bristol generally decreases from north to south. According to He et al. [16], an analysis of the functional loss of Bristol's road network under flood conditions indicated that the northern areas are not prone to flooding and are unaffected by

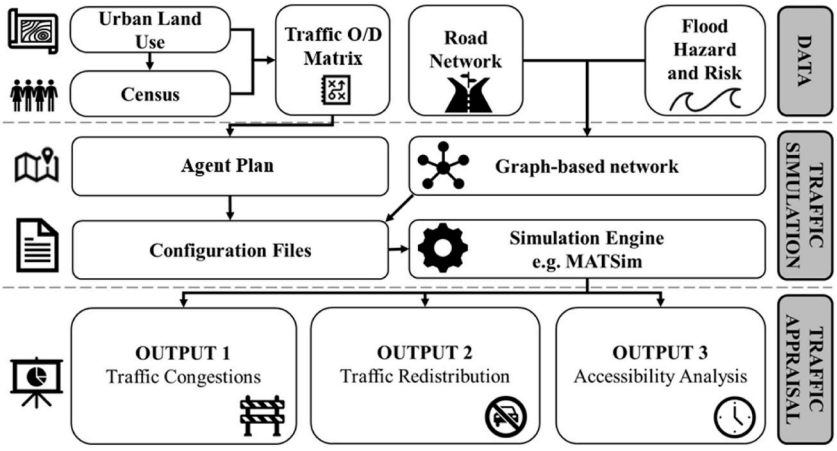

Fig. 1. Methodological workflow.

Table 1
Configuration of the input data.

Dataset	Source	Spatial res. & CRS	Preprocessing steps	Citation
Road network topology (graph)	OpenStreetMap (via OSMnx); OpenStreetMap Foundation (≈2020 edition cited); Boeing [66]	Vector (nodes/links); CRS as per manuscript; clipped to central Bristol	OSM tag filters → link attribute mapping (free speed, capacity, lanes); conversion to MATSim	[19,66]
Building footprints & land-use proxies	OpenStreetMap buildings/land use data	Vector polygons; CRS as per manuscript	Select relevant building categories; classify into residential, academic, and commercial	[19]
Car ownership statistics	Bristol City Council – Bristol Key Facts 2023	City vehicles statistics data	Adopt city-level share as constraint for agent car availability	[67]
Flood hazard/ intensity	Fathom	Raster with 10 × 10 m resolution	LISFLOOD-FP layers provide the maximum inundation depth for each return period	[41]
Vehicle fragility/ depth–speed	Vehicle stability experiment in flood from literature; fragility convolution [42]	No spatial (parameter curves)	Vehicle experimental data and normal distribution support to vehicle fragility	[31,42]
Zoning grid & OD matrices	Derived from the building polygons and local population assumptions	Grid resolution: 400 x 400 m	Grid creation; building-to-zone allocation; gravity model OD with exponential decay	[68]

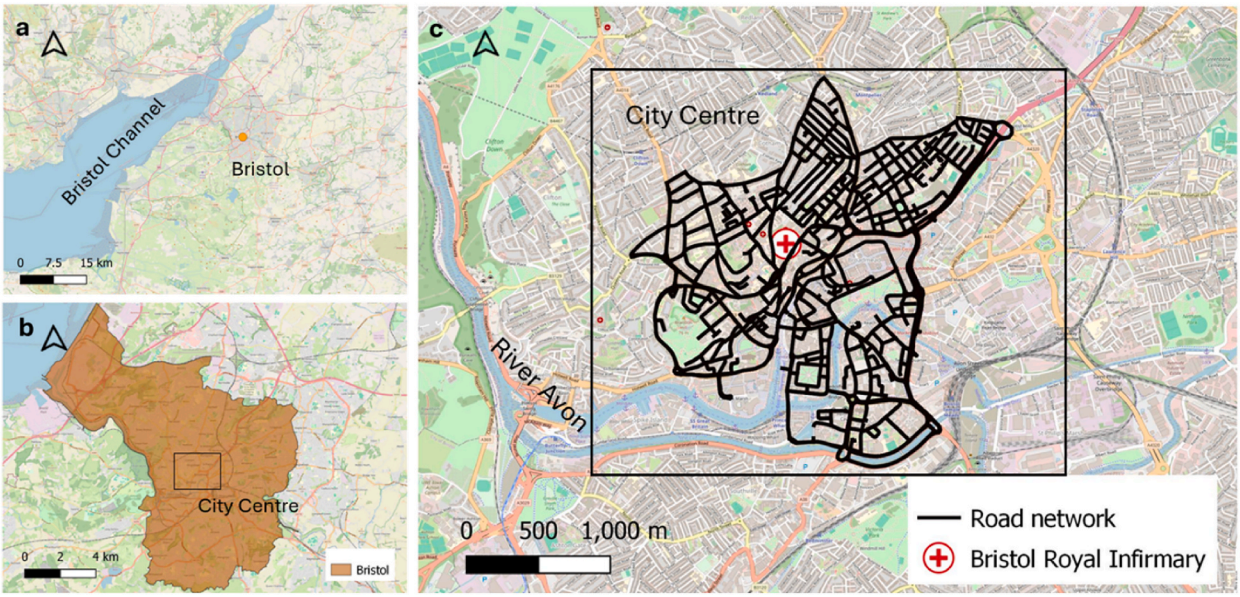

Fig. 2. The geographical layout of Bristol; (a) geographical location of Bristol and the Bristol Channel; (b) geographical distribution of Bristol and the location of the city centre; (c)road network layout of central Bristol and the course of the River Avon.

floodwaters from the River Avon. Therefore, to assess traffic congestion before and after flood-induced network disruptions, the study area was reduced in size. The analysis focused on the city centre region near the River Avon, as shown in Fig. 3. This spatial reduction preserves the representativeness of road traffic flow while significantly decreasing the computational cost, thereby enabling a more efficient and timely simulation of congestion impacts. On this city-centre network (≈3.37% of the Bristol administrative area), a full-day MATSim simulation with 250 iterations required about 6 h on a standard workstation. Scaling to the full municipal network would be considerably more computationally expensive, and it has been deemed unnecessary for BRI-focused accessibility appraisal. The study area encompasses arterial roads, local streets, and river-crossing links, and includes a hospital situated in the city centre. This combination of road types and central siting provides an appropriate setting for analysing flood impacts on urban road traffic. In this study, major roads refer to arterial routes in the city centre with higher free speeds and capacities. In contrast, minor roads denote local streets with lower capacities.

This study examines the functional characteristics of the road network using lane counts and free speeds, utilising a combination of satellite imagery (e.g., Google Maps) and field data. The loss of road network functionality due to flooding is modelled by reducing the free speed of affected links using the approach proposed by He et al. [43]. This approach provides a practical, continuous representation of flood-induced disruptions to road performance.

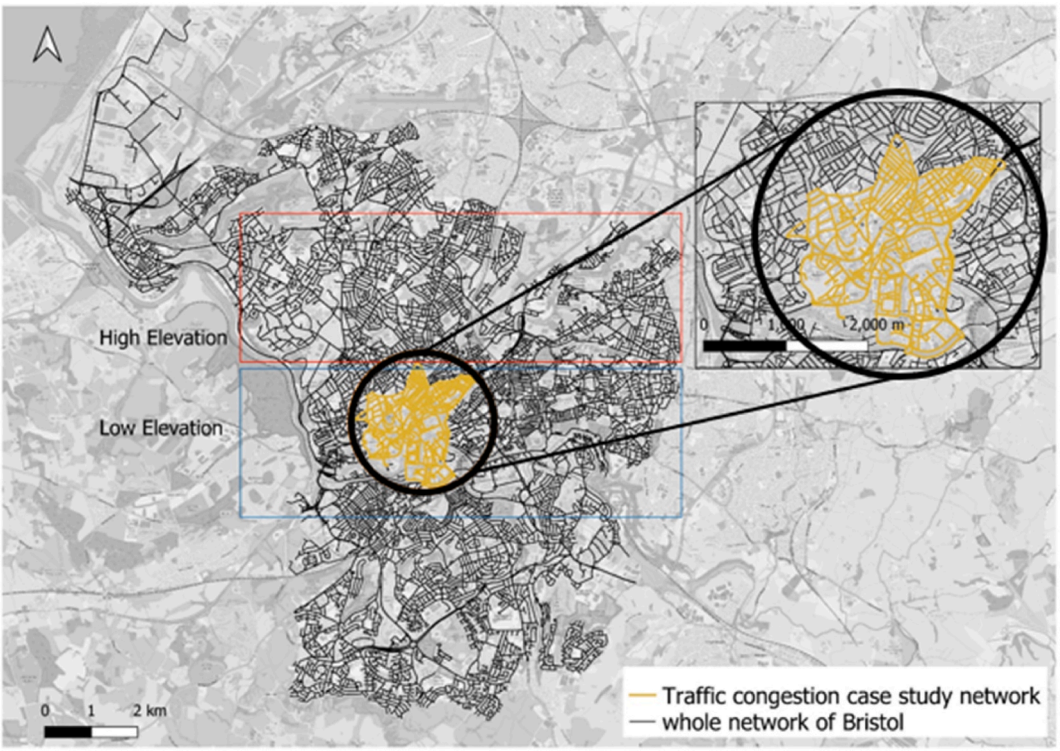

Fig. 3. Case study area for traffic congestion analysis in Bristol.

3.3. Flood hazard and risk

The second dataset consists of flood hazard and consequent probabilistic functionality risk. Flood hazard data include measures such as flood depth and velocity, which can affect the performance of the road network. In this study, rather than developing a new risk model, we adopt the probabilistic functionality framework developed by He et al. [43], which assesses the probability of vehicle instability during flooding and maps it to obtain the likelihood of functional loss across the road network. Following De Risi et al. [42] and the implementation in He et al. [43], the mean annual rate (λ_{LS}) of exceeding a specific limit state (i.e. vehicle instability) is obtained by convolving the flood hazard curve (intensity versus frequency) with the vehicle fragility curve, as shown in Equation (1).

$$\lambda_{LS} = \int_0^{v_f} P(LS|v_f) \cdot \left| d\lambda(v_f) \right| \tag{1}$$

where $P(LS|v_f)$ describes the vehicle fragility curve, and $|d\lambda(v_f)|$ denotes the absolute value of the differential of the flood hazard curve expressed in terms of flood velocities v_f.

Equations (2) and (3) show the derivation of $P(LS|v_f)$ and $\lambda(v_f)$.

$$P(LS|v_f) = \phi\left(\frac{\log(v_f) - \eta}{\beta}\right) \tag{2}$$

$$\lambda(v_f) = K_0 \times {v_f}^K \tag{3}$$

where $\phi()$ is an operator representing the Cumulative Distribution Function (CDF) of a normal distribution. η and β are the logarithmic mean value and standard deviation, respectively. In this study, the median value represents the flood velocity a vehicle can withstand at the specified flood depth. The logarithmic standard deviation is calculated by studying the residuals of the fitted experimental data. In the flood hazard curve, the K_0 and K are two parameters obtained by fitting flood intensity vs flood return periods. By integrating flood risk into the road network topology, road attributes can be modified to examine their influence on traffic dynamics. Specifically, $P(LS) = 1 - \exp(-\lambda_{LS} \cdot t)$ can be used to alter the free speed of each inundated link. The simulations evaluate two conditions: the baseline network and a risk-impaired network. This comparison provides a general assessment of network vulnerability, congestion hotspots, and accessibility impacts without considering a specific scenario (e.g. return period).

All hazard-curve and fragility parameters (μ, σ, K_0, K) and the resulting link-level mean annual rates λ_{LS} are taken directly from the calibration and validation reported in He et al. [43]; the novelty of the present study lies in how these probabilistic link-level risks are

translated into speed reductions and embedded within the agent-based traffic simulation

3.4. OD matrix and Agent's plan

Agents' plans represent the travel patterns of all agents within the road network, defined by their origin–destination (OD) pairs. In this study, agents' plans are determined using urban land-use and census data. Urban land use refers to the spatial distribution of various types of buildings within a city. The type of building defines the nature of agent activities; for example, residential buildings are associated with home activities, while commercial buildings are associated with work activities. An agent travelling from home to work generates a specific OD pair within the transport network. The OD matrix is an input derived from land-use and census data using the gravity model. Each OD pair is then instantiated as discrete MATSim agents with daily plans, so the simulation is executed entirely at the agent level. This approach aligns with literature [69] that treats the road network as a 'reservoir' and agents as 'inflows' and 'outflows,' facilitating a balance between spatial flexibility and agent-based dynamics.

Previous studies collected agent movement data using sensors, GPS, and social media, enabling precise tracking of individual travel behaviours [59,70,71]. However, these methods face two key limitations: ethical concerns about collecting sensitive mobility data and the high financial and logistical demands of large-scale data collection. This study employs an alternative approach that does not require the direct tracking of individual movements, enabling the rapid estimation of agents' daily activities and overall traffic flow within the road network (see Sec. 3.4.1).

3.4.1. Overview of agent plan synthesis approach

The approach follows six key steps to generate travel demand and assess mobility dynamics (Fig. 4):

(1) Construct a buffer around the network (the grey areas in Fig. 4(a)) to identify areas in which agents are likely to depart from and travel to.

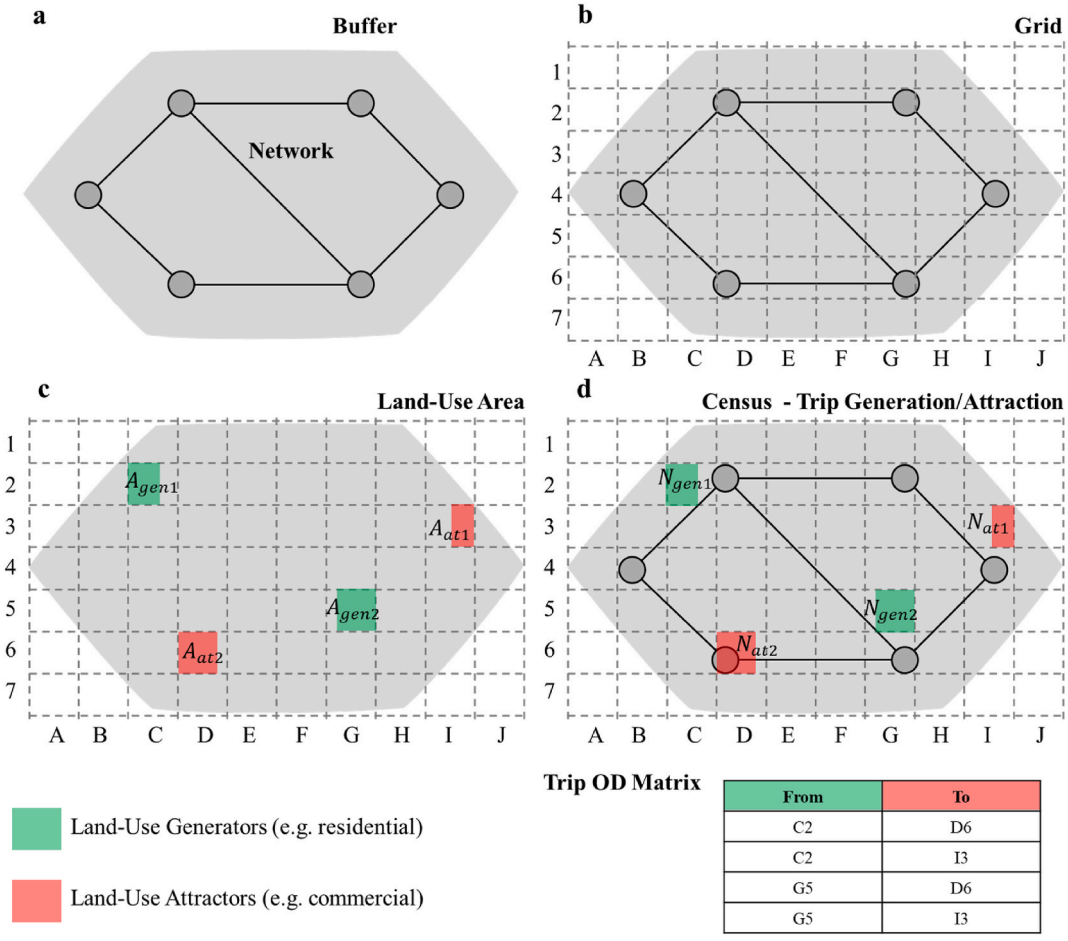

From	To
C2	D6
C2	I3
G5	D6
G5	I3

Fig. 4. Schematic process of predicting traffic patterns and generating OD matrices: (a) network buffer and zoning, (b) grid overlay, (c) land-use mapping, and (d) trip generation, attraction and OD matrix assembly.

(2) Create a regular grid on the buffer (shown in Fig. 4(b)).
(3) Map the different urban land uses (residential building footprint, commercial building footprint, etc.) to each grid in the buffer zone (shown in Fig. 4(c)).
(4) Allocate population census data to each zone based on the proportion of residential urban land use area.
(5) Estimate the trip generation and trip attraction of each zone according to the urban land use footprint and census (shown in Fig. 4(d)).
(6) Utilise a gravity model to randomly allocate the travel OD matrix, with travel distance acting as the impedance factor.

A buffer zone is constructed around the road network to define candidate origins and destinations for inter-zone trips, as shown in Fig. 4(b); the specific choice of buffer width is described in Section 3.5.

For each zone, the footprint area of the different urban land uses is measured. The census population within the buffer area is allocated to each zone based on the area of the residential footprint within that zone, representing the potential number of trips generated by each zone. Commercial and other non-residential regions are used to approximate trip attraction potential (Fig. 4(c)). Similarly, the number of trips attracted by non-residential buildings is determined by the area of their building footprints, reflecting factors such as job density. If a zone contains both residential and non-residential land, it functions as both a trip generator and a trip attractor. Thus, each zone is associated with both trip generation and trip attraction values. Finally, a gravity model is applied, using inter-zone distance as an impedance factor, to distribute trips between zones based on trip generation and attraction rates, thereby capturing the spatial distribution of travel demand and generating the OD matrix (Fig. 4(d)). In this study, greater distances between trip generation and attraction zones result in lower attraction strength and fewer agents travelling between them; agents are not assigned with trips within the same zone.

3.4.2. Trip generation and attraction methods

Trip generation for each zone assumes that agents depart from home to engage in activities such as work or shopping. Specifically, the trip generation and trip attraction for each zone are calculated using Equations (4) and (5), respectively, with parameter assumptions detailed in Section 3.5.

$$N_{gen,i} = A_{gen,i} \cdot \alpha \cdot \frac{n_v}{a_i} \tag{4}$$

$$N_{at,j} = \sum_{j=1}^{n} A_{at,j} \cdot \frac{1}{a_j} \tag{5}$$

where $N_{gen,i}$ represents the number of trips generated within a given zone of area $A_{gen,i}$. The α represents the proportion of households owning a vehicle. The n_v and a_i are the average number of vehicles per household and the average residential footprint area per household, respectively. In the trip attraction, the $N_{at,j}$ represents the total number of trips attracted by all zones. $A_{at,j}$ and a_j represent the non-residential building footprint area of each zone and the area required per agent for non-residential activities. In this study, both trip generation and attraction are rounded up to the next larger whole number; for example, 1.2 is treated as 2.

3.4.3. Gravity model formulation

The gravity model allocates trip generation from each zone to other zones according to distance decay and zone-specific attraction factors [65]. This cross-allocation process enables the construction of an OD matrix, capturing agents' travel patterns between zones. Equation (6) [65] represents the calculation of trip distribution within zones using the raw gravity model. Here, T_{ij} is the number of trips from the zone i to zone j, α_{cali} is a calibration parameter, and $f(d_{ij})$ is a distance impedance function defined in Equation (7), where C denotes the friction factor. t_{ij} is the estimated number of trips originating from the zone i to zone j within a defined period, and the n is the total number of destination zones in the study area.

$$T_{ij} = \alpha_{cali} \cdot N_{gen,i} \cdot N_{at,j} \cdot f(d_{ij}) \tag{6}$$

$$f(d_{ij}) = \frac{C}{(t_{ij})^n} \tag{7}$$

While the raw gravity model (Equation (6)) can overpredict flows and requires calibration of scaling factors, the normalised gravity model overcomes this limitation by ensuring probabilistic consistency and conservation of total trip productions. Moreover, the normalised form has been demonstrated in transportation studies to produce more reliable trip distributions under constrained conditions [72]. Therefore, in this study, a constrained normalised gravity model is employed to estimate the OD matrix, ensuring that each generated trip is assigned to a destination zone. Distance acts as the impedance parameter, assuming that agents preferentially select the nearest suitable destination for their travel purpose. Consequently, the number of the trip from zone i to zone j are modelled using a constrained normalised gravity model (Equation (8)), which incorporates building footprints and travel distance impedance [68].

$$T_{ij} = \frac{N_{gen,i} \cdot N_{at,j} \cdot f(d_{ij})}{\sum_k (N_{at,k} \cdot f(d_{ik}))} \tag{8}$$

$N_{at,k}$ represents trip attraction of the destination zone k and $f(d_{ik})$ is the corresponding distance impedance function from the zone i to zone k. As the power-law function in Equation (7) is more commonly applied to large-scale migration studies, it may be less appropriate for urban-scale analysis. Since this study focuses on an urban city centre, an exponential decay form (Equation (9)) is therefore adopted, as it better captures short-to medium-distance travel and allows straightforward calibration of the decay parameter γ [68].

$$f(d) = e^{-\gamma d} \tag{9}$$

where d is the Euclidean distance between origin and destination, and γ is the decay parameter controlling the sensitivity to distance. In practice, a decay parameter $\gamma = 0.001$ was chosen, as it provides a sufficiently steep distance decay to capture proximity preference in urban-scale commuting, while remaining computationally stable and consistent with values used in previous spatial interaction studies (e.g., Ref. [73]).

While this method provides an approximate representation of individual agents' travel origins and destinations, it effectively captures the overall spatial distribution of traffic flows by accounting for travel costs. This approach is especially valuable in the absence of detailed agent-level travel data, offering a practical means to analyse trip patterns at an aggregate scale.

3.5. Trip generation and attraction assumptions

In this study, a 900-m buffer is established around the road network to define the zoning system for OD matrix generation, following Gil's [74] pragmatic recommendations. This buffer width represents a compromise that retains approach links to the hospital while avoiding unnecessary enlargement of the study area and keeping the analysis focused on hospital-oriented accessibility.

Consistent across official sources, Census 2021 data published by ONS in 2023 and Bristol City Council's Bristol Key Facts 2023 both report similar car availability in Bristol: approximately 74% of households have at least one car/van and 26% have none (equivalently 73.8% vs 26.2% in the ONS table) [67,75]. We therefore assume 74% (≥1 car/van) and 26% (no car/van) as the constraint on agent car availability in Equation (4). Based on Howden Insurance's (2023) analysis of Bristol's Census 2021 data, 50,141 households reported no car, 87,781 owned one, 41,397 owned two, and 12,321 owned three or more. For modelling parsimony, we apply a proportional allocation and assume an average of approximately one vehicle per household.

As described in Section 3.4, residential building footprints are used to allocate population to zones. The same footprints also proxy the spatial distribution of vehicle ownership, allowing zone-level vehicle totals to be inferred and then used to estimate trip generation using the average vehicle-per-household assumption above. To bound the analysis, we adopt a conservative worst-case assumption that all car-owning households travel by car, thereby approximating maximal congestion conditions.

In addition to vehicle ownership, Equation (4) requires an estimate of the average household footprint area. Given the large number and varied types of households, determining individual household footprints is highly challenging. According to the Average UK House Size statistics [76], the most common residential building types include apartments (~60 m^2), bungalows (~77 m^2), terraced homes (~82 m^2), semi-detached homes (~100 m^2), and detached homes (~150 m^2). In this study, the number of stories is also considered,

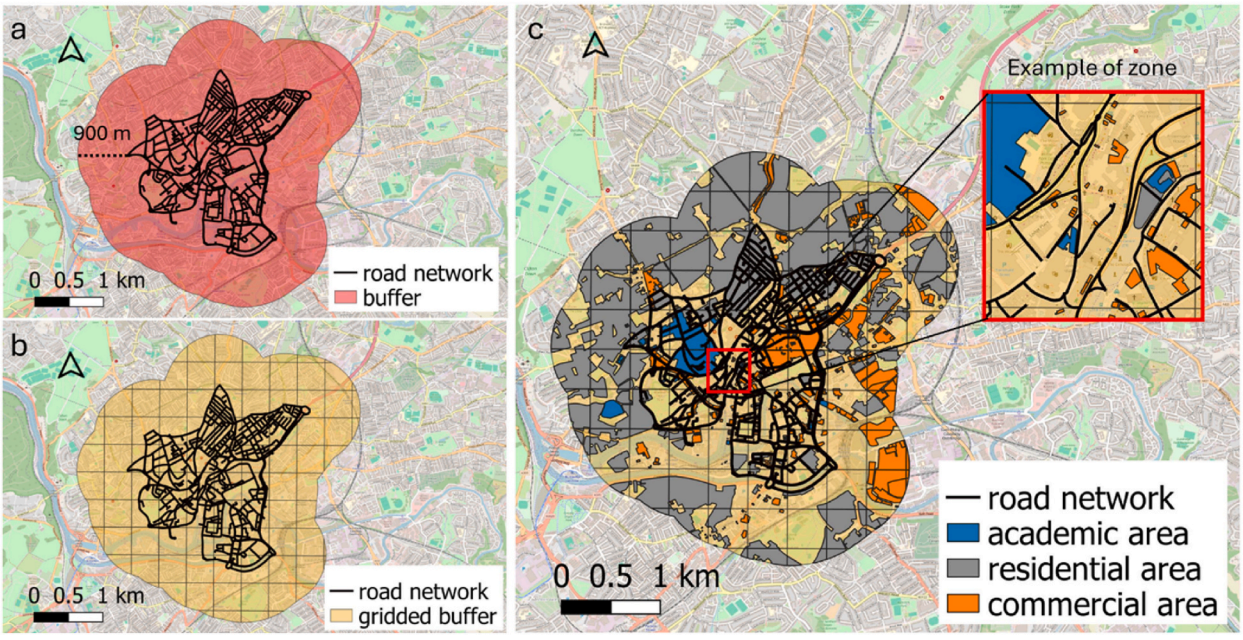

Fig. 5. Process of determining trip generation and attraction for each zone: (a) buffer created based on the case study road network; (b) buffer divided into zones using a grid; (c) buildings allocated to zones according to grid boundaries.

and after averaging across housing types, the mean household footprint is approximated as 100 m^2. This approximation (≈100 m^2) is consistent with official UK housing statistics reporting typical dwelling floor areas at this scale (DLUHC, 2022; [77]). With average household footprint and vehicle ownership data, Equation (4) enables the calculation of trip generation per unit area.

In addition to residential land use, this study also considers other key land use types, such as academic and commercial areas. These locations typically represent common destinations for daily activities and are therefore important indicators of trip attraction. According to the definition of trip attraction in Equation (5) of Section 3.4, the first step involves identifying building types within the buffer area. In this study, the relevant (non-residential) building types include academic areas, commercial areas, office buildings, and street-facing shops. Building footprint data are extracted from OpenStreetMap, and average floor area assumptions are applied for trip attraction estimations. For practically, non-residential buildings are grouped into two categories: academic (study) and non-academic (work) facilities (including commercial areas, office buildings, and street-facing shops). Campus planning practices typically allocate approximately 100 m^2 per staff member including buildings and surrounding facilities [78], and retail-space standards indicate a range of 15–75 m^2 per person [79]. Accordingly, this study applies 100 m^2 per academic job and 40 m^2 per commercial job. Based on the proportion of each zone's footprint allocated to these land uses, trip attraction is calculated and aggregated.

Yu et al. [80] analysed traffic flows in Beijing using 1000 m and 500 m grids and demonstrated that smaller zones capture land-use variation more accurately. Given the compact study area, a 400 m grid balances spatial detail with computational efficiency; larger cells (500–1000 m) would merge heterogeneous blocks and reduce OD accuracy, while smaller cells would add unnecessary complexity. It also preserves short trips and local routing, enabling the MATSim OD matrix to reflect realistic urban demand under flood conditions. Consistent with this finding, this study adopts a 400 m grid, which is considered appropriate for Bristol's city-centre road network as it preserves the finer urban structure while keeping the simulation tractable. (Fig. 5(b)). All buildings within the buffer are assigned to individual zones based on their spatial location relative to zone boundaries (Fig. 5(c)).

For each zone, trip generation and attraction values are calculated and then assembled into an OD matrix between zones, which is subsequently used as input for the MATSim simulation.

3.6. Traffic simulation

Traffic within the road network is simulated using MATSim (see Sec. 2). In MATSim, the *configuration* setup serves as the central input for running simulations of agents' dynamic traffic behaviour. The *configuration* setup incorporates two essential input datasets: the *Graph-based network* (Section 3.2) and the *Traffic OD Matrix* (Section 3.4), which include the road network topology and agents' travel plans, respectively. To isolate flood effects on congestion and hospital-oriented accessibility, travel demand is held fixed across baseline and flood scenarios (i.e., no trip cancellations or departure-time shifts).

The MATSim simulation is configured using four main modules in *configuration*: *controler*, *qsim*, *planCalcScore*, and *strategy*. The *controler* module defines the overall simulation process, the *qsim* module manages queue-based traffic flow simulation. The *planCalcScore* module specifies utility-based scoring rules to evaluate agents' travel plans, while the *strategy* module governs plan selection and adaptation [81]. All parameters are configured following standard MATSim practice, with full details provided in Section 4. Agents are assumed to have perfect knowledge of flood-induced link impairments and prevailing traffic conditions and, at each iteration, replan routes; accordingly, this idealised information setting provides an upper bound on congestion redistribution.

3.7. Traffic congestion and redistribution

Following the dynamic traffic simulation in MATSim, traffic congestion and the redistribution of traffic across the road network can be analysed and described as follows.

3.7.1. Traffic congestion

In this study, traffic congestion is approximated as the ratio (R) of an agent's travel speed (V_a) to the corresponding link's free speed (V_0), as defined in Equation (10). However, MATSim does not capture the real-time travel speed of agents, and the instantaneous speeds of vehicles on a link vary. Therefore, this study first calculates the average speed of each agent travelling a link in a given time window (Equation (11)), where l_j is the length of the given link j, and t_{i-in} and t_{i-out} are the timestamps for the agent i entering and exiting the link j, respectively. n is the total number of agents who travel through the link j. The detailed classification of congestion within the road network is presented in the results of Section 4.1.

$$R = V_a / V_0 \tag{10}$$

$$V_a = \frac{1}{n} \sum_{i=1}^{n} \frac{l_j}{t_{i-out} - t_{i-in}} \tag{11}$$

3.7.2. Traffic redistribution

The second part of the analysis focuses on the traffic redistribution within the road network under various damage scenarios. Redistribution reveals the flow of traffic as routes adjust in response to disruptions, providing valuable insights for predicting congestion patterns following a disruption. In this study, the traffic redistribution is evaluated as the speed ratio of agent travel (R_s) before (V_{a-1}) and after (V_{a-2}) the functional disruption of the road network, as defined in Equation (12).

$$R_s = V_{a-2}/V_{a-1} \tag{12}$$

Although the speed ratio can offer a preliminary insight into traffic redistribution, it does not account for changes in the network's free speed due to functional disruption. Since the free-flow speed may vary before and after flood, observed changes in actual speeds are based on shifting free-flow speed conditions. Consequently, relying solely on actual speed ratios may introduce bias.

To more accurately assess traffic redistribution, this study uses a *redistribution ratio*, which compares the ratio of actual speed to free-flow speed under different network states rather than comparing actual speeds directly, as shown in Equation (13). $\overline{R}$ represents the redistribution ratio, with R_1 and R_2 denoting the actual-to-free-flow speed ratios before and after disruption.

$$\overline{R} = \frac{\left(\frac{V_{a-2}}{V_2}\right)}{\left(\frac{V_{a-1}}{V_1}\right)} = \frac{R_2}{R_1} \tag{13}$$

3.7.3. Agent count ratio

To validate the accuracy of the speed ratio and redistribution ratio, and to more intuitively reflect the inflow or outflow of vehicles on links before and after the loss functionality, this study also employs the agent count ratio. This ratio is defined as the quotient of the number of agents on a link before the functional loss to that after the loss, as expressed in Equation (14).

$$R_c = N_1/N_2 \tag{14}$$

where R_c is the agent count ratio. N_1 and N_2 are the agent numbers for the road network before and after functionality loss.

3.7.4. Critical assessment of the three indicators

Although all three indicators describe redistribution effects, they are distinct yet complementary. The speed ratio captures the direct operational impact on travel speeds, the redistribution ratio evaluates how far actual performance diverges from design capacity, and the agent count ratio quantifies the magnitude and direction of traffic shifts across the network. Together, they provide complementary insights into post-flood dynamics.

For the three ratios (defined respectively by agents' travel speed, the ratio of travel speed to free-flow speed, and changes in agent counts on each link before and after flooding) the interpretation is consistent. When a ratio exceeds 1, it indicates that fewer agents used the link after flooding, which naturally results in higher travel speeds for those remaining; conversely, a ratio below 1 reflects an inflow of agents detouring from other disrupted links, leading to increased load on the affected road. These variations capture the redistribution of traffic within the network, hereafter referred to as "redistribution". For ratios below 1, thresholds of 0.8 and 0.6 were adopted and standardised into three bands following Level-of-Service principles: values above 0.8 indicate a limited inflow of agents to the link, values between 0.8 and 0.6 represent a moderate level of inflow, and values below 0.6 capture heavy inflows of agents detouring from other disrupted links, leading to unstable traffic conditions and pronounced redistribution effects. Speeds under 60% of free-flow speed were grouped into a single interval down to zero, since further subdivision provides little practical distinction under urban flood conditions. To ensure consistency, these thresholds were uniformly applied across all three ratios, with detailed classification tables reported in Appendix A.

3.8. Accessibility analysis

To evaluate road network efficiency, this study uses a time-based isochrone method, which estimates travel times from a defined origin to all other zones. This approach captures the spatial distribution of accessibility across the network. A time-based isochrone defines the area reachable within a given travel time from a specific location, reflecting the functional accessibility of the transport system [82]. Because agents with the same OD pair may follow different paths, travel times from a specific zone to other zones are computed as the mean across all such agents and used to construct the isochrone.

Unlike conventional models that assume free-flow speed conditions, this method accounts for vehicle interactions and congestion, providing a more realistic representation of travel times. In MATSim, agents are dynamically reassigned to alternative routes to alleviate congestion. meaning that even those with identical OD pair may experience different travel times. To reflect this variability, the mean travel time of all agents with the same OD pair is used to generate the corresponding isochrone. This procedure enables the identification of zones with reduced accessibility due to congestion and provides insights into performance under varying demand and disruption scenarios.

The simulation is conducted at the zonal level (see Section 3.5), with each zone being treated as a unit. All locations within a zone share the same isochrone, ensuring consistency in accessibility representation. Travel times are then compared across zones before and after flood-induced loss of functionality, highlighting temporal changes in accessibility patterns. For the case study, the zone containing Bristol Royal Infirmary is selected as the origin, and time-based isochrones with 2, 4, 6 and 8 min thresholds are generated; the 8-min band reflects current UK ambulance response guidelines [82–84], allowing accessibility to be interpreted in terms of emergency response coverage.

4. Results

The simulation experiments are implemented in MATSim using the case study network, OD matrix, and flood-induced functional loss parameters described in Section 3.3. In this application, the flood is considered in a static manner; the hazard and traffic modules are decoupled. The iteration was set to 250, which sensitivity checks showed was sufficient to reach a stable adaptive equilibrium (agents' plans, link flows, and travel-time distributions showed no change beyond this point). All simulation parameters for iterations, scoring coefficients, and agent replanning strategies are summarised in Table 2; such parameters are chosen to balance behavioural realism with stable convergence. These follow standard MATSim practice, with calibration values selected to strike a balance between realistic congestion formation and computational stability. A minimal runnable example and configuration files are provided in Appendix B to support reproducibility. Two network states are modelled:

1. Baseline: non-flood; full network functionality.
2. Flood: free-flow speeds are reduced on inundated links according to the hazard–vulnerability method of He et al. [43].

The analysis focuses on congestion patterns measured by the congestion identification, traffic redistribution assessed through the speed ratio, redistribution ratio and agent count ratio, and accessibility changes evaluated using time-based isochrones. Classifications for interpreting these ratios, along with their corresponding tables, are presented in the subsections below in Section 3.

In terms of computational performance, with the current road network size and agent population fixed, a full. MATSim run with 250 iterations required about 6 h to complete. Increasing the iterations to 400 extended the runtime to approximately 11 h. In both cases, the system reached equilibrium, where agent route choices stabilised and no further changes occurred between iterations, indicating that either setting is sufficient for convergence. However, the substantial increase in runtime highlights how sensitive computational costs are to iteration count alone, even without enlarging the network or agent population. For this reason, 250 iterations were adopted to ensure that the analysis remains both computationally efficient and robust for rapid flood impact assessment. All runs were executed on a Dell laptop with an Intel® Core™ i7-10850H @ 2.70 GHz and 16 GB RAM; higher-spec hardware would proportionally reduce the reported wall-clock times.

4.1. Traffic congestion analysis

Congestion levels are quantified using Equation (10), and their classification is presented in Table 3 based on the full 24-h MATSim simulation. As MATSim operates on a daily time scale, congestion outcomes are derived from the cumulative travel behaviour of all agents over the course of the day. Accordingly, the impaired free-speed parameters remain fixed throughout the daily simulation to represent a one-year observation window. Assuming no overtaking occurs during agent travel within the road network, this study uses the functional loss associated with the highest-risk vehicle (i.e. cars) (see Fig. 6). According to He et al. [43], cars pose the highest risk during flood events among vehicle types. This approach ensures a conservative estimation of network performance under flood-induced disruptions.

The thresholds in Table 3 are based on the 'Level of Service' principles commonly used in traffic studies [87]. Values above 0.9 indicate conditions close to free-flow speed, while those between 0.9 and 0.8, and between 0.8 and 0.6, represent increasing delay but generally stable flow. Ratios below 0.6 capture unstable conditions where congestion intensifies rapidly, and traffic performance breaks down [87]. In Fig. 6, the percentages are calculated over the risk-exposed network—i.e., the total extent of road links shown in red (rather than over the number of roads or the full network). Across the ten classes, the three upper bands (0.45–0.61, 0.61–0.90, and 0.90–3.50% annual probability) together comprise about 58% of the risk-exposed network, with the largest single share in 0.45–0.61% (~29%). Lower-risk classes each occupy smaller shares (e.g., 0.06–0.15% ≈ 10%), consistent with elevated risk clustering along riverside secondary streets and bridge approaches. Higher-risk links cluster along riverside secondary streets and bridge approaches,

Table 2
MATSim simulation parameters and configuration.

Module	Parameter (italic in text)	Definition/Behavioural role	Value
Controler	*iterations*	Number of iterations until agents' travel plans converge to equilibrium	250 (tested; equilibrium is achieved)
PlanCalcScore	*learningRate*	Determines the rate at which agents adapt their travel behaviour across iterations	0.6 [85]
PlanCalcScore	*BrainExpBeta*	Level of randomness in their decision-making process	2.0 [85]
PlanCalcScore	*lateArrival*	Penalty applied when agents arrive later than the preferred time	−18.0 [85]
PlanCalcScore	*earlyDeparture*	Penalty applied when agents depart earlier than the preferred time	0
PlanCalcScore	*performing*	Utility of performing an activity (e.g. home, work, education)	6 [85]
PlanCalcScore	*waiting*	Utility assigned when agents are idle or waiting	0
PlanCalcScore	*marginalUtilityOfTraveling*	Disutility per unit of time spent travelling	−10.0
PlanCalcScore	*marginalUtilityOfDistance*	Disutility per unit distance	−1.0
PlanCalcScore	*moneyDistanceRate*	Conversion rate between monetary cost and distance	0
Strategy	*BestScore*	Method used to evaluate and retain the agent's "best" plan	0.1 [86]
Strategy	*ReRoute*	Generation of alternative routes in response to current network dynamics	0.9 [86]
QSim	*startTime, endTime*	Defines the start and end time of the simulation period	00:00–24:00 h

Table 3
Traffic congestion classification.

R	Congestion classification
1 – 0.9	No congestion
0.9 – 0.8	Minor congestion
0.8 – 0.6	Moderate congestion
0.6 – 0 (not included)	Severe congestion
0	Not used

Fig. 6. The road network risk map in the annual observation flood (from Ref. [43]).

while city-centre arterials set back from the River Avon generally exhibit lower risk. This spatial pattern anticipates the subsequent shift of congestion from riverside corridors to higher-capacity centre arterials once flooded links lose functionality (Fig. 7).

Fig. 7 shows the traffic congestion map of Bristol. The analysis focuses on two specific areas of the road network (Fig. 7(a)), for illustrative purposes. According to the road network design in Bristol, Area 1 comprises major roads in the city centre, located away from the River Avon. Area 2 includes minor roads near the River Avon. As boundary roads facilitate the ingress and egress of agents from regions outside the buffer area, their congestion levels are excluded from the analysis. Under baseline flood-free conditions (Fig. 7 (b) and (d), baseline scenario), most roads within the network remain uncongested; however, noticeable congestion still occurs on several minor roads in Area 2 (Fig. 7(d)), primarily due to their role as key river crossings. Roads within Area 2 are noticeably more congested than those in Area 1 (Fig. 7(b)), since they serve as key connections between both sides of the river. In the absence of network functionality loss, MATSim prioritises shorter routes over detours. Consequently, these roads experience high traffic volumes, resulting in significant congestion. Although the roads in Area 1 are in the city centre and carry higher traffic volumes, they are classified as major roads with higher free speeds and capacities than those in Area 2. As a result, under conditions without network functionality loss, these roads do not exhibit significant congestion, as shown in Fig. 7(b).

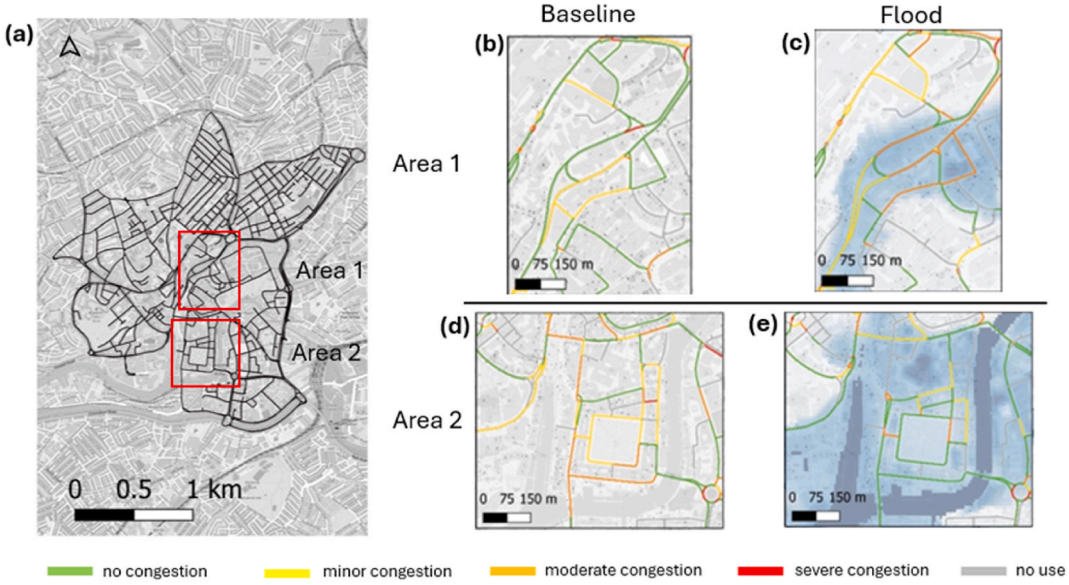

Fig. 7. Traffic congestion maps of the road network for both baseline and flood scenarios of Area 1 and Area 2; (a) The research road network and geo-location of two case study areas; (b) traffic conditions of Area 1 under baseline condition; (c) traffic conditions of Area 1 under flood condition; (d) traffic conditions of Area 2 under baseline condition; (e) traffic conditions of Area 2 under flood condition.

When flooding occurs (Fig. 7(c) and (e)), congestion in Area 1 (Fig. 7(c)) significantly worsens, whereas congestion in Area 2 (Fig. 7 (e)) eases due to the diminished functionality of roads in Area 2. As a result, a larger number of agents divert their travel to less affected major roads in Area 1, increasing traffic flow, reducing average speeds, and intensifying congestion. While roads in Area 2 remain partially useable, fewer agents opt to use them, instead preferring to avoid delays by selecting alternative routes. Compared to pre-flood conditions, the traffic load on Area 2 decreases. Despite reduced performance, the remaining vehicles in Area 2 generally travel close to the downgraded free speeds, leading to a spatial shift in congestion from Area 2 to Area 1.

To compare baseline and flooded conditions in Areas 1 and 2, this study computes (per area) the proportion of activated road links in each congestion class and the aggregate congested (minor–severe) to uncongested link ratio. Fig. 8(b) shows the aggregate split between uncongested and congested (minor–severe) links: Area 1 shifts from 61% uncongested/39% congested at baseline to 33%/67% under flood, whereas Area 2 moves from 28%/72% at baseline to 58%/42% under flood. Fig. 8(a) details the composition of classes: in Area 1, no congestion drops to about half its baseline share, minor rises slightly, and moderate approximately doubles, while severe remains nearly unchanged, indicating a flood-induced redistribution that loads bridge approaches and central connectors, worsening local operating conditions. In Area 2, congestion increases sharply during flooding, and all congested classes decline, consistent with a loss of priority and reduced inflow to this largely minor-road subnetwork once traffic is rerouted to higher-capacity corridors. Operationally, these shifts imply that flood-triggered functional loss concentrates demand onto Area 1's primary links (requiring targeted management), while de-loading Area 2.

4.2. Agent redistribution and potential congestion

The analysis of congestion under varying disruption scenarios in Section 4.1 demonstrates that congestion patterns within the road network are not static. To better understand the dynamics of these changes, this study applies the travel speed ratio and redistribution ratio defined in Section 3.4 to analyse link-level responses to flooding.

4.2.1. Agent travel speed ratio

Using the methods outlined in Equations (6) and (7) in Section 3.4, the average travel speed of all agents on each link is calculated, allowing the derivation of the speed ratio before and after the disruption in network functionality. Fig. 9 illustrates the ratio of agent travel speeds before and after the flood-induced disruption to network functionality.

In Fig. 9, most links in Area 1 exhibit a travel speed ratio between 0 and 1, suggesting a reduction in average agent speed after the disruption in network functionality. This decline implies that these roads became more congested in the post-disruption scenario, as they absorbed additional traffic following the flood and overall movement slowed. Unlike Area 1, Area 2 demonstrates a reverse pattern, where agent travel speeds on numerous links increased after the flooding. This pattern reflects a decline in the functional capacity of these roads, rendering them less attractive for route selection within the MATSim simulation. As a result, a significant portion of traffic was rerouted away from Area 2, reducing the number of agents traversing its links. With decreased traffic volumes, the remaining vehicles experienced improved flow conditions, leading to higher speeds and speed ratios exceeding one. These results suggest that post-flooding, there is a notable shift in route choice towards roads in Area 1, as agents systematically avoided flood-impacted and functionally compromised links to reduce their travel time. These results are representative of active traffic management. This trend further implies that the main roads within Bristol's city centre may be subject to heightened traffic demand under flood conditions, thereby imposing additional strain on the central transport infrastructure.

4.2.2. Redistribution ratio

To isolate the effect of flood-induced changes in free speed, this study uses the redistribution ratio defined in Equation (13) (Section 3.4), which compares the ratio of actual speed to free speed on each link before and after the disruption. Fig. 10 presents the spatial distribution of redistribution ratios across the road network.

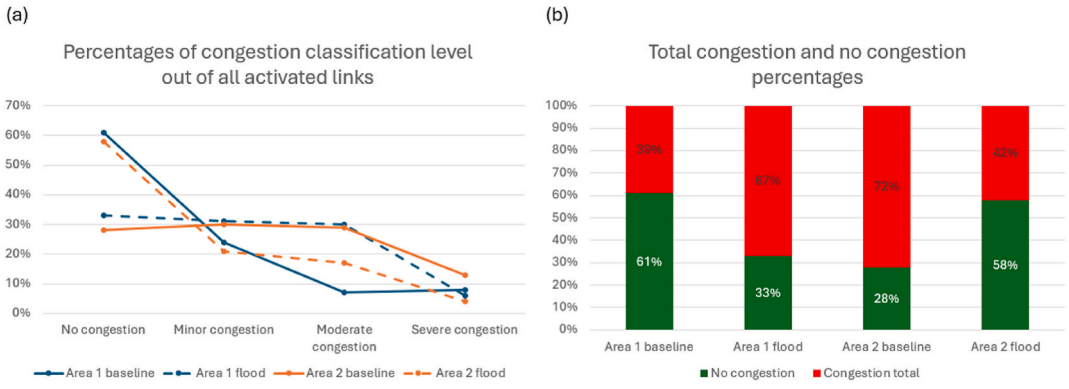

Fig. 8. Congestion composition by area and scenario; (a) share of activated links in each congestion class for Area 1 and Area 2 under baseline and flood conditions; (b) aggregate split of congested (minor–severe) versus uncongested links for each area and scenario.

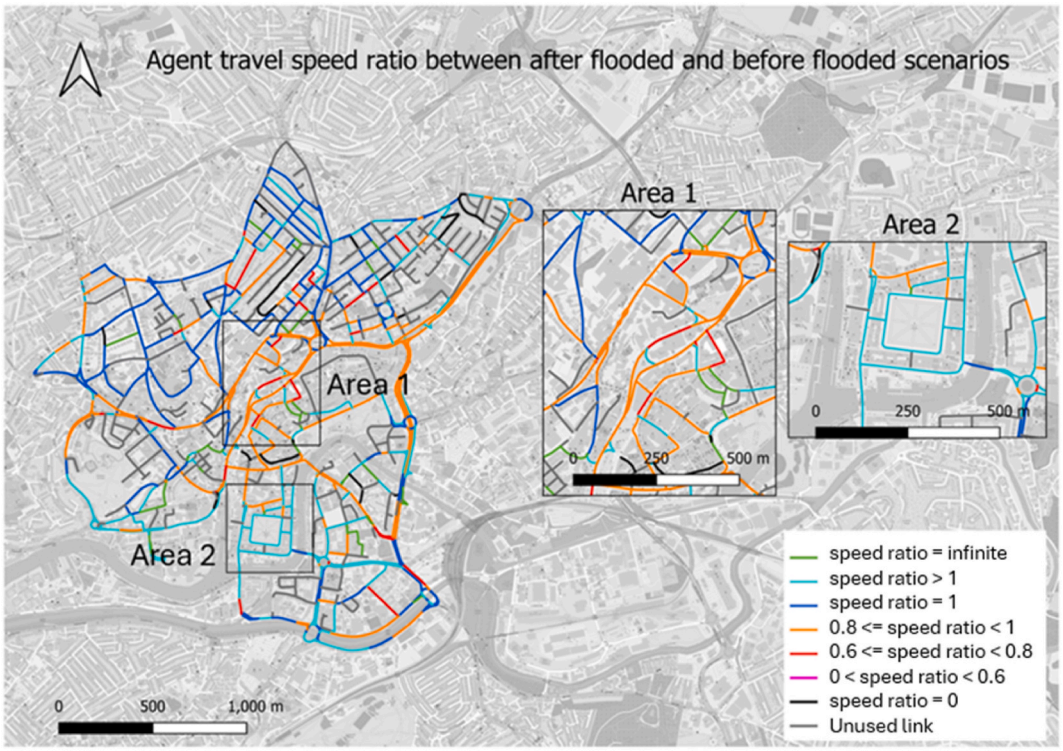

Fig. 9. Spatial distribution of agent travel speed ratios before and after disruption.

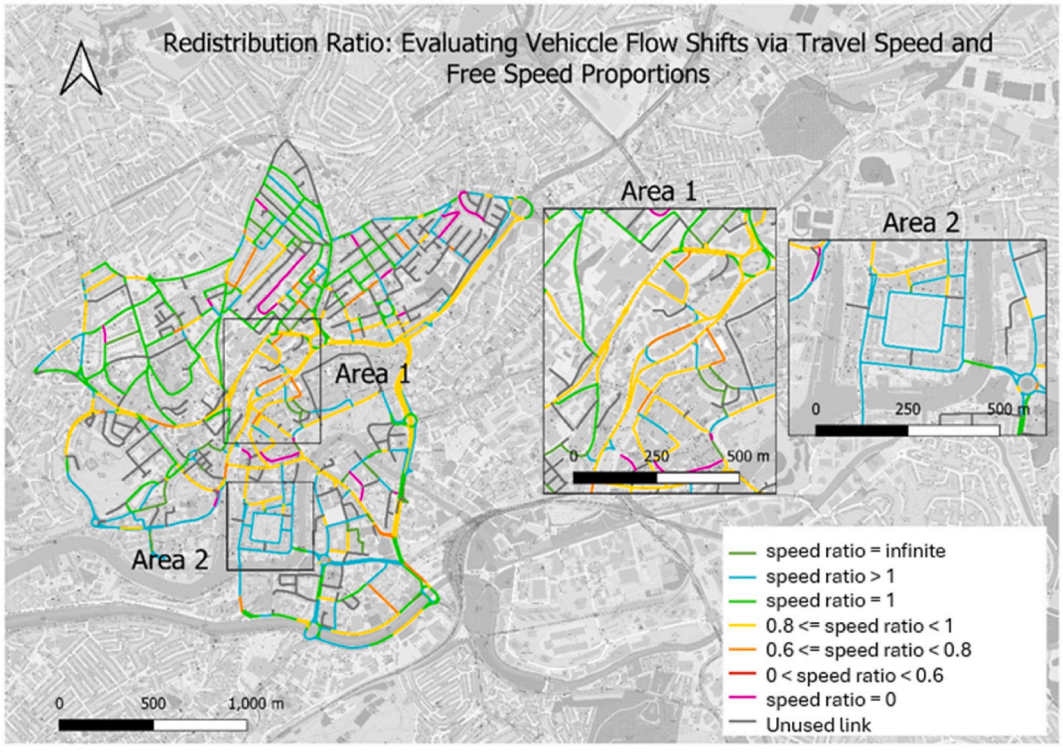

Fig. 10. Spatial distribution of redistribution ratios before and after network disruption.

Similarly, the layout of redistribution ratios in Area 1 and Area 2 is analysed following flood disruption. As shown in Fig. 10, in Area 1, most road links exhibit redistribution ratios between 1.0 and 0.8, with a smaller proportion falling within the 0.8-0.6 range. This result indicates that, following the flood-induced degradation of network functionality, the difference between agent travel speeds and the corresponding free speeds on these roads has widened. The findings suggest that a significant number of vehicles were rerouted from other roads to the major routes in Area 1. This diversion leads to increased traffic volumes and subsequently reduced travel speeds on these main roads.

Conversely, most roads in Area 2 display redistribution ratios exceeding 1, suggesting that the gap between agent travel speeds and corresponding free speeds narrowed following flood-induced disruptions to the road network. This pattern implies fewer obstacles to traffic flow, as these routes are deprioritised by agents in response to the reduced functionality. As a result, agents divert away from Area 2, decreasing local congestion and allowing vehicles that remained to travel at speeds closer to the free-flow speed conditions.

Compared to the distribution of agent travel speed ratios, the redistribution ratio shows consistent spatial patterns. Both results indicate that following flood-induced disruptions to the road network, vehicle speeds in Area 2 increased, reflecting reduced congestion. In contrast, vehicle speeds in Area 1 decreased, suggesting heightened congestion in this area. These findings indicate that, in Bristol, flood-induced disruptions to the road network led to increased vehicle concentration on unaffected primary roads, resulting in higher traffic volumes and pressure. This redistribution may contribute to congestion in Area 1, highlighting a rising trend in traffic delays following functional losses in the road network due to flooding.

4.2.3. Agent count ratio

To complement the speed-based indicators, this study also examines the agent count ratio defined in Equation (14) (Section 3.4), which compares the number of agents on each link before and after the disruption. This number provides a direct check on redistribution patterns inferred from the speed ratio and redistribution ratio. Fig. 11 presents the distribution of agent count ratios before and after the loss of road network functionality.

In the aftermath of the flooding, Area 1 experiences a marked rise in vehicle presence across almost all roads, indicating that traffic redistributes from other regions toward this area. Conversely, Area 2 shows a general decline in vehicle numbers on most streets, indicating that it no longer serves as a preferred route and that traffic is diverted elsewhere. These observations, when considered alongside the agent speed ratio and redistribution ratio, confirm the directional shifts in agent movement caused by the disruption. The agent count ratio provides further insight into the reasons behind link-level speed changes, illustrating whether these changes stem from increases or decreases in traffic volume. These changes in vehicle distribution contribute to increased congestion, slower travel speeds, and heightened delays on primary routes.

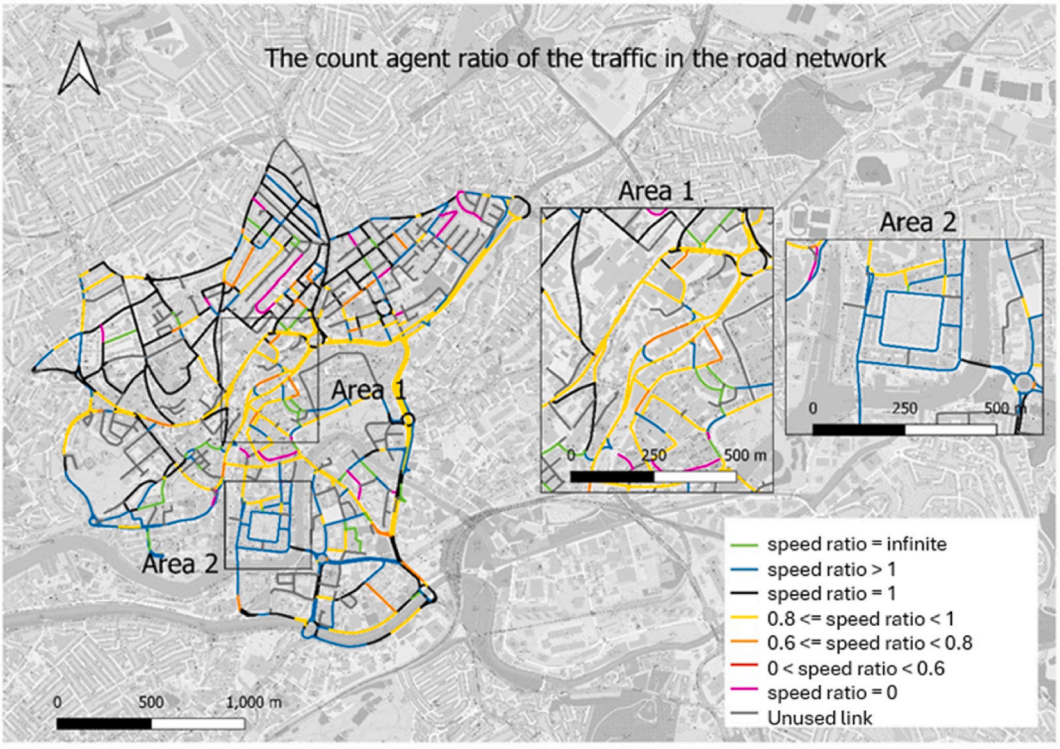

Fig. 11. Spatial distribution of agent count ratios before and after network disruption.

4.3. Time-based isochrone Area

Considering the Bristol Royal Infirmary (BRI) as origin, Fig. 12 compares pre- and post-flood travel-time bands across the study area building on the BRI-centred isochrones defined in the accessibility analysis for 2, 4, 6 and 8 min (Section 3.6).

Fig. 12(a) and (b) illustrate the travel times from BRI to other zones before and after the loss of road network functionality, respectively. Regardless of whether the road network retains full functionality, Fig. 12 clearly indicates that areas to the north of the BRI remain more accessible within the same travel time bands. This enhanced accessibility is attributed to the hospital's position along key arterial routes that extend northward, offering greater connectivity and structural redundancy. Conversely, the southern network comprises predominantly minor roads with limited redundancy and is further hindered by the river, which restricts movement and diminishes reachability.

A comparison of time-based isochrones before and after the loss of road network functionality reveals a consistent reduction in isochrone coverage across 0-2 min and 2-4 min travel time thresholds, indicating a decline in vehicle speeds around the BRI. The increased coverage of the 4–6 and 6–8 min isochrones indicates that congestion-induced reductions in vehicle speed cause areas that would otherwise be reachable within shorter travel times to require longer journey times. The flooding scenario causes travel times in certain areas of the study region to exceed 8 min, particularly in the southern part of the network. This increase is primarily due to detours taken by vehicles to avoid flooded roads, which extend travel distances and durations. Additionally, the disruption creates new congestion near Bristol Royal Infirmary, further delaying emergency response. The limited redundancy of roads extending southward from the hospital, combined with the necessity of crossing the river, exacerbates travel delays in the affected areas.

These results underscore the profound influence of traffic redistribution, induced by the loss of road network functionality, on spatial accessibility. Crucially, when major or arterial roads experience sudden surges in traffic, and critical infrastructure such as hospitals is situated along these routes, even slight disruptions to network function can cause severe reductions in accessibility. For emergency vehicles, the influx of other traffic onto arterial roads surrounding the hospital increases congestion and adversely affects their accessibility. However, it should be noted that roads experiencing reduced flow due to rerouting could, in principle, offer less congested alternatives for emergency vehicles, although the overall loss of accessibility to the hospital often outweighs such benefits.

To compare accessibility with and without congestion, the study simulates agent's BRI-centred isochrones of MATSim dynamic simulation and static simulation under flooded conditions across the same time frames. For comparability, the static simulation isochrones were clipped using the same buffer as the traffic simulations, as shown in Fig. 13(a). Fig. 13(b) illustrates, for the flooded scenario, the MATSim-simulated isochrones of vehicles departing from BRI at each timeframe. Within the same buffer, contractions of nearer-timeframe isochrones are compensated by expansions in longer-timeframe bands. Within the 0–2 and 2–4 min isochrones, the areal extent of the MATSim-simulated isochrones is markedly smaller than that of the static simulation. This indicates that congestion in the road network is already propagating from the vicinity of BRI, thereby degrading traffic performance across the wider network. Comparing the 4–6 and 6–8 min isochrones between the MATSim dynamic simulation and the static simulation shows that the dynamically simulated isochrones are substantially larger than their static counterparts. This result indicates that congestion forces areas that would otherwise be reachable within shorter travel times to be accessed only after longer journeys, such that the 4–6 and 6–8 min bands in the dynamic case now cover zones reached by shorter travel-time bands in the static scenario. An additional 8–10 min isochrone also emerges in the MATSim dynamic simulation but is absent in the static simulation, demonstrating that, once congestion is accounted for, accessibility from BRI deteriorates markedly and reductions in network efficiency originate in the immediate vicinity of BRI.

4.4. Agent-based traffic simulation validation

To validate the MATSim representation of network traffic, modelled baseline (no-flood) travel times from BRI to each zone are

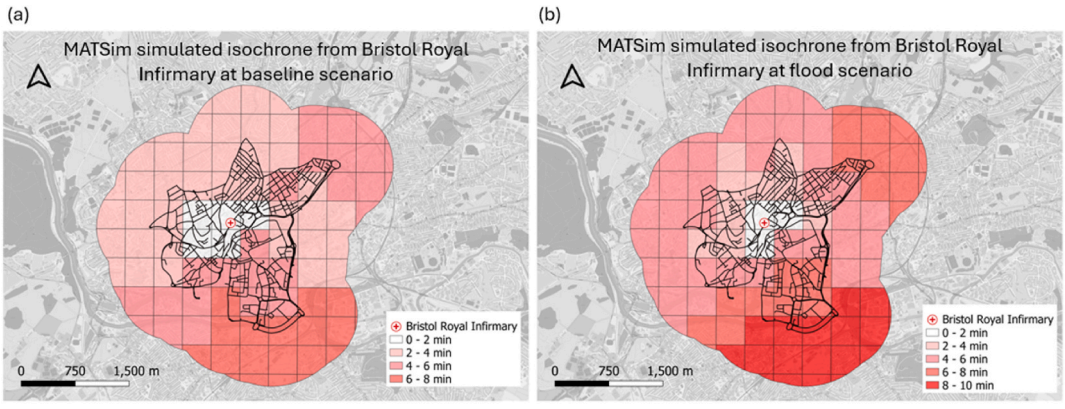

Fig. 12. The time-based isochrone areas from Bristol Royal Infirmary; (a) the isochrone at baseline scenario without the road network functionality loss; (b) the isochrone at flood scenario with the road network functionality loss.

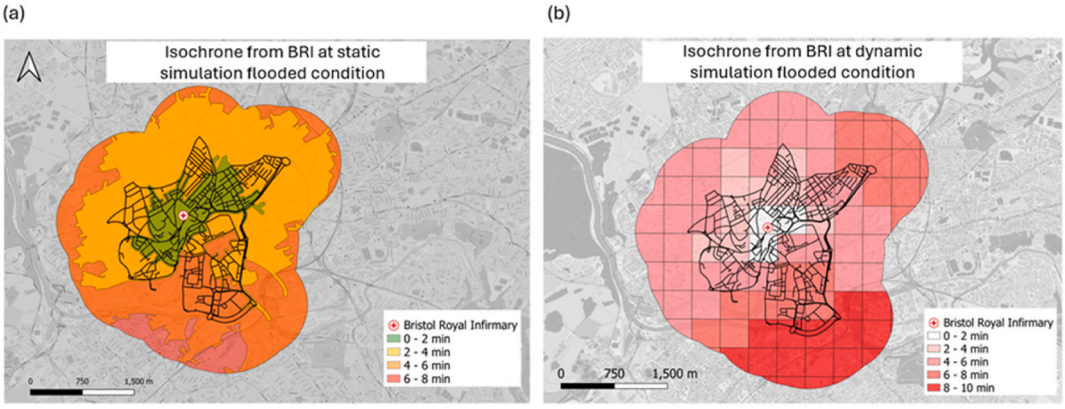

Fig. 13. Isochrone comparison between static simulation and MATSim dynamic simulation (BRI-centred) at flooded condition; (a) isochrone via static simulation; (b) isochrone via MATSim dynamic simulation.

compared with corresponding Google Maps estimates from BRI to each zone. Due to independent-scenario-based simulation, historical flood-event observations cannot be used for validation.

Fig. 14(a) shows the absolute difference between Google Maps and MATSim travel times from BRI by zone (Google Maps travel time vs MATSim travel time): 0 min denotes exact agreement, 0–2 min, 2–4 min, and 4–6 min denote increasing deviation bands. Fig. 14(b) shows that 0 min accounts for 31.29% of zones. Although the time variation of 0–2 min (32.29%) and 2–4 min (32.29%) bands exceed the 0 min share, the 0 min zones spatially span the road-network footprint, indicating that where zones overlap the network the simulated times are consistent with observed estimates. By contrast, zones not overlapping the network connect via virtual links, which shorten access and yield systematic underestimation relative to Google Maps; the time variation of 4–6 min cluster in the southern buffer arises from zones across the river. In the fact, the travel which needs to cross the river needs more time than the direct connected virtual link. Overall, the validation indicates that the chosen MATSim parameters reproduce realistic travel times for network-overlapping zones, with discrepancies increasing as zone–network separation grows.

5. Discussion

This research reveals that flooding impairs the operational capacity of the road network, leading to congestion on affected routes. Since congestion evolves dynamically, vehicles tend to adjust their paths to avoid slower segments, thereby redistributing traffic to other parts of the network and potentially creating additional bottlenecks. The MATSim platform proves effective in modelling these changes by simulating route shifts and mitigating overall congestion through dynamic traffic assignment. Case studies focusing on roads in the city centre and areas adjacent to the river, both highly vulnerable to flooding, offer insights into patterns of congestion and traffic redistribution. Additionally, time-based isochrones are utilised to evaluate accessibility under baseline and flood travel conditions, highlighting the consequences of congestion. The primary conclusions are summarised as follows:

(1) Under baseline conditions, flood-susceptible roads in Area 2 experienced higher congestion than those in the city centre (Area 1); however, this pattern reversed under flooding conditions. Flood-induced functional loss on non-arterial roads in Area 2 prompted vehicle redistribution toward less-affected arterial routes in the city centre. The resulting surge in traffic volume on these main roads led to reduced travel speeds and intensified congestion, indicating that flooding poses a significant risk of increased congestion within central Bristol.
(2) Traffic congestion across the network compromises the accessibility of emergency vehicles leaving Bristol Royal Infirmary. In particular, rerouting vehicles due to impaired network performance substantially alters the overall accessibility pattern. This impact is especially pronounced when travelling between Bristol's northern and southern zones, where extended journey times are observed.

Although this study successfully simulated and analysed congestion within the road network, several limitations must be acknowledged. Firstly, agent activities were inferred from building functions and simplified to include only work-related trips, which fails to capture the complexity and diversity of actual travel behaviour involving multiple activity types. In practice, travel behaviour is frequently trip-chained and multi-purpose (e.g., home→work→shopping/childcare→other activities→home), so restricting agents to work trips overlooks these combined patterns. Secondly, agent numbers were estimated from building footprints, and trip patterns were generated using a gravity model. While helpful in outlining overall flows between zones, this method lacks the precision to represent individual movement patterns and the inherent variability in behaviour. These assumptions may be refined in future research as more detailed spatial and demographic data become available. Thirdly, the dynamic model excluded key elements, such as traffic signal delays and overtaking, and assumed uninterrupted vehicle flow. However, vehicles encounter signal delays and overtaking, so this idealised assumption may bias travel times and, especially for ambulances, the extent of reachable isochrone areas.

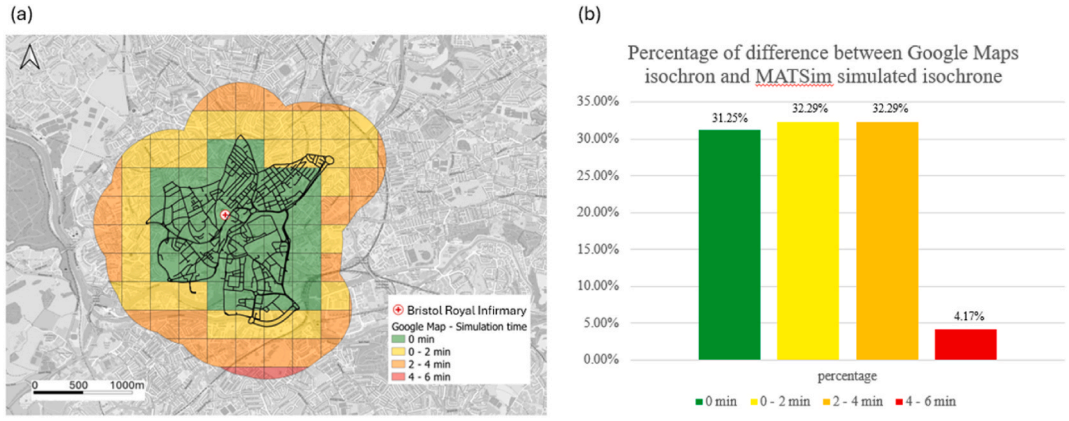

Fig. 14. Baseline isochrone validation (BRI-centred); (a) the time difference between the Google Maps and MATSim simulation map; (b) the histogram of each time difference classification percentage out of all zones.

Additionally, the study assumes that drivers possess perfect knowledge of the network, traffic, and disruptions. In practice, however, drivers often rely on habitual routes and imperfect, outdated information, so they may remain on congested links, making the model's travel-time and accessibility results somewhat optimistic relative to real-world conditions. Fourthly, travel was represented using zonal grids, which define trips between zones rather than between specific nodes, thereby limiting the resolution of traffic flow analysis and underrepresenting fine-scale dynamics. Fifthly, while agents within a buffered area of the network were considered, those outside the buffer could still contribute to traffic within the study area, potentially leading to an underestimation of volume and, consequently, travel times. Furthermore, our study considered only car travel within the road network, whereas in reality vehicle types are far more complex. However, this limitation can be addressed in future studies by incorporating experimental data on the flood vulnerability of known vehicles.

Despite these constraints, the model is adaptable to various urban contexts. By conceptualising the road network as a “reservoir” and agents as “inflows” and “outflows”, it allows flexible spatial adjustments. It simplifies behavioural assumptions by focusing on the number of users rather than the details of their activities. Unlike conventional models that assume free-flow conditions, this method accounts for vehicle interactions and congestion, providing a more realistic representation of travel conditions. In MATSim, agents are dynamically assigned to alternative routes to reduce congestion. As a result, even agents with the same OD pair may take different paths and experience different travel times. Future studies could enhance the model's accuracy by incorporating more granular OD data to reflect actual traffic patterns better. Although the case study is centred on Bristol, the novelty of the framework lies in its ability to evaluate not only congestion under baseline conditions but also the emergence of potential hotspots following traffic redistribution when the network is flooded. This transferability enables the framework to be applied across diverse urban morphologies and network structures, while maintaining its focus on accessibility and resilience assessment.

5.1. Future work

Building on the above limitations and strengths, several targeted extensions could improve fidelity and decision usefulness. First, enhance activity–travel realism by moving beyond work-only trips to represent trip-chaining and multi-purpose tours with schedule constraints (e.g., work→shopping/childcare→home). Second, incorporate network operations (signal control, turn delays, overtaking) and test emergency-vehicle priority (e.g., signal pre-emption), quantifying impacts on ambulance isochrones under disruption. Third, overcome the assumption of perfect knowledge by modelling habitual routing, bounded rationality, partial awareness of closures, and adaptive learning. Fourth, increase spatial resolution from coarse zone-to-zone flows to node–link/path-level dynamics, and run sensitivity analyses on grid size and gravity-decay parameters to quantify the effects of resolution. Fifth, strengthen data and calibration by fitting OD patterns and route choice to observed datasets (GPS/mobile/trajectory sensors) and reporting uncertainty bounds. Sixth, mitigate boundary effects by coupling the study area to a wider regional demand model or dynamic inflow profiles to capture flood-induced rerouting. Finally, represent hazard dynamics and recovery explicitly by linking traffic capacity to time-varying flood/dewatering trajectories and reopening schedules to capture evolving impacts.

5.2. Policy implications

This study couples hazard mapping of flood intensity with link-level functional transportation potential loss and agent-based traffic simulation, yielding outputs directly actionable for preparedness, response, and recovery. In particular, the framework produces (i) congestion/redistribution maps that reveal where flows concentrate after link degradation, (ii) link-specific performance metrics (percentage functional loss) for targeting interventions, and (iii) time-based isochrones from a critical facility (Bristol Royal Infirmary, BRI) to quantify accessibility under disruption. These products translate technical findings into operational signals for emergency management, transport operations, and strategic policy.

The agent-based approach captures behavioural rerouting and network-wide redistribution, enabling scenario-specific evacuation and access planning. The approach allows for the representation of a complex real-world situation by explicitly modelling interactions among vehicles, buildings, and floodwater, where decisions interact in non-linear ways, and their consequences are difficult to anticipate. Isochrone analyses identify time-critical catchments for ambulance dispatch and hospital access under varying flood severities, supporting: (a) pre-positioning of emergency resources, (b) protected ambulance corridors (e.g., bridge approaches and inner-city arterials), and (c) event-time traffic control (signal retiming, temporary lane control, reversible lanes) to preserve emergency travel times. Because the method outputs link-level loss as percentages, agencies can set trigger thresholds (e.g., when functional loss on a bridge approach exceeds x%, activate detours A/B). This study demonstrates the potential of agent-based modelling through a case study. By accounting for factors typically absent from empirical models, such as individual characteristics (e.g., age), building construction types, and the road network, it could become a crucial tool for rescue operations and evacuations.

6. Conclusion

This study developed and applied a novel framework to evaluate traffic congestion and accessibility loss caused by flood-induced functional disruption in urban road networks. The methodology integrated three key components: flood hazard data, road network exposure, and vehicle vulnerability, represented through link-level changes in free-flow speed. By employing a probabilistic flood risk model and linking it to road functionality loss, the study developed a dynamic, nuanced simulation of flood impacts on traffic flow. MATSim was used to simulate travel patterns and agent-based route adjustments before and after flood-induced network degradation. Key congestion metrics (travel speed ratios, redistribution ratios, and agent count ratios) were analysed to identify spatial patterns of vehicle rerouting. The simulation focused on central Bristol, a flood-prone city characterised by complex topology and a riverine environment.

The results revealed a significant shift in congestion from flood-prone secondary roads next to the river to major arterial roads in the city centre following flood events. This redistribution led to reduced travel speeds and increased traffic congestion on central corridors. The time-based isochrone analysis further demonstrated the reduction of accessible areas, especially south of the River Avon, highlighting reduced reachability for emergency services operating from Bristol Royal Infirmary. The findings emphasise the importance of accounting for both spatial traffic redistribution and functional network degradation in flood impact assessments. By capturing how agent route choices evolve in response to network conditions, the model identifies not only immediate congestion but also longer-term accessibility risks. This research contributes to proactive urban flood risk management by informing adaptive planning and resilience strategies. The model identifies how congestion hotspots shift before and after flooding and shows that these shifts severely reduce the isochrone-based accessibility of vehicles departing from Bristol Royal Infirmary. Policy measures should therefore prioritise safeguarding and upgrading these critical corridors, for example, through targeted drainage improvements, prioritised maintenance, or temporary traffic restrictions to keep emergency routes clear. Operational guidelines could also include predefined detour plans and dynamic traffic management strategies to preserve hospital accessibility during flood events.

CRediT authorship contribution statement

Ke He: Writing – original draft, Visualization, Validation, Software, Methodology, Investigation, Formal analysis, Conceptualization. **Neil Carhart:** Writing – review & editing, Supervision, Methodology. **Maria Pregnolato:** Writing – review & editing, Visualization, Supervision. **Raffaele De Risi:** Writing – review & editing, Supervision, Methodology, Data curation, Conceptualization.

Declaration of competing interest

This manuscript is the authors' original work and has not been published or submitted elsewhere. The research presented accurately reflects the authors' analysis and findings, with all sources properly cited and acknowledged. All authors have contributed significantly to the conception, design, execution, and interpretation of the study, and each accepts responsibility for the content. The authors declare that they have no known competing financial interests or personal relationships that could have appeared to influence the work reported in this paper.

Acknowledgement

Flood hazard data were provided by Fathom, Bristol. Ke He and Raffaele De Risi acknowledge support from the project Community and Infrastructure Resilience to Climate-geological Long-term Effects (CIRCLE), ES/Z000122/1.

Appendix A. Supplementary data

Supplementary data to this article can be found online at https://doi.org/10.1016/j.ijdrr.2026.106053.

Data availability

The data that has been used is confidential.

References

[1] N. Zhang, A. Alipour, Integrated framework for risk and resilience assessment of the road network under inland flooding, Transp. Res. Rec.: J. Transport. Res. Board 2673 (12) (2019) 182–190, https://doi.org/10.1177/0361198119855975.

[2] M. Pregnolato, A. Ford, S.M. Wilkinson, R.J. Dawson, The impact of flooding on road transport: a depth-disruption function, Transport. Res. Transport Environ. 55 (2017) 67–81, https://doi.org/10.1016/j.trd.2017.06.020.

[3] D. Lu, S.L. Tighe, W.-C. Xie, Impact of flood hazards on pavement performance, Int. J. Pavement Eng. 21 (6) (2020) 746–752, https://doi.org/10.1080/10298436.2018.1508844.

[4] N. Matini, S. Gulzar, S. Underwood, C. Castorena, Evaluation of structural performance of pavements under extreme events: flooding and heatwave case studies, Transp. Res. Rec.: J. Transport. Res. Board 2676 (5) (2022) 1–11, https://doi.org/10.1177/03611981221077984.

[5] Q. Chen, Z. Zhang, K. Gaspard, Case study on the impact of flooding and inundation on pavement performance, Transp. Res. Rec.: J. Transport. Res. Board 2677 (3) (2023) 1–10, https://doi.org/10.1177/03611981231152247.

[6] K. Pyatkova, A.S. Chen, S. Djordjević, D. Butler, Z. Vojinović, Y.A. Abebe, M. Hammond, Flood impacts on road transportation using microscopic traffic modelling techniques, Lect. Notes Math. (2018) 115–126, https://doi.org/10.1007/978-3-319-33616-9_8.

[7] L. Abdulla, M.M. Morsy, A.J. Kalyanapu, Modeling temporal accessibility of an urban road network during an extreme pluvial flood event, Nat. Hazards Rev. 23 (4) (2022) 04022027, https://doi.org/10.1061/(ASCE)NH.1527-6996.0000586.

[8] A.A. Rajput, S. Nayak, S. Dong, A. Mostafavi, Anatomy of perturbed traffic networks during urban flooding, Sustain. Cities Soc. 97 (2023) 104693, https://doi.org/10.1016/j.scs.2023.104693.

[9] F. Jalayer, R. De Risi, F. De Paola, M. Giugni, G. Manfredi, P. Gasparini, M.E. Topa, N. Yonas, K. Yeshitela, A. Nebebe, G. Cavan, S. Lindley, A. Printz, F. Renner, Probabilistic GIS-based method for delineation of urban flooding risk hotspots, Nat. Hazards 73 (2014) 975–1001, https://doi.org/10.1007/s11069-014-1119-2.

[10] R. De Risi, F. Jalayer, F. De Paola, Meso-scale hazard zoning of potentially flood prone areas, J. Hydrol. 527 (2015) 316–325, https://doi.org/10.1016/j.jhydrol.2015.04.070.

[11] Z. Kalantari, M. Cavalli, C. Cantone, S. Crema, G. Destouni, Flood probability quantification for road infrastructure: Data-driven spatial-statistical approach and case study applications, Sci. Total Environ. 581–582 (2017) 386–398, https://doi.org/10.1016/j.scitotenv.2016.12.147.

[12] R. De Risi, F. Jalayer, F. De Paola, S. Lindley, Delineation of flooding risk hotspots based on digital elevation model, calculated and historical flooding extents: the case of Ouagadougou, Stoch. Environ. Res. Risk Assess. 32 (6) (2017) 1545–1559, https://doi.org/10.1007/s00477-017-1450-8.

[13] R. De Risi, F. Jalayer, F. De Paola, S. Carozza, N. Yonas, M. Giugni, P. Gasparini, From flood risk mapping toward reducing vulnerability: the case of Addis Ababa, Nat. Hazards 100 (1) (2019) 387–415, https://doi.org/10.1007/s11069-019-03817-8.

[14] K. He, R. De Risi, M. Pregnolato, N. Carhart, J. Neal, Graph-based framework for road network performance and flood risk assessment, in: 14th International Conference on Applications of Statistics and Probability in Civil Engineering, 2023, pp. 1–7. Dublin; ICASP14.

[15] K. Pyatkova, A.S. Chen, D. Butler, Z. Vojinovic, S. Djordjevic, Assessing the knock-on effects of flooding on road transportation, J. Environ. Manag. 244 (2019) 48–60, https://doi.org/10.1016/j.jenvman.2019.05.013.

[16] K. He, M. Pregnolato, N. Carhart, J. Neal, R. De Risi, Functionality assessment of road network combining flood roadworthiness and graph topology, Transp. Res., Part D Transp. Environ. (2024) 104354, https://doi.org/10.1016/j.trd.2024.104354, 104354.

[17] W. Kron, Flood risk = Hazard × exposure × vulnerability, Int. Assoc. Hydro-Environ. Eng. Res. (2002). https://www.iahr.org/library/infor?pid=16216.

[18] H. Zhang, C. Li, J. Cheng, Z. Wu, Y. Wu, A review of urban flood risk assessment based on the framework of hazard-exposure-vulnerability, Prog. Geogr. 38 (2) (2019) 175–190, https://doi.org/10.18306/dlkxjz.2019.02.003.

[19] OpenStreetMap Foundation, OpenStreetMap, Retrieved from, https://www.openstreetmap.org/about, 2020.

[20] G.P. Cimellaro, A.M. Reinhorn, M. Bruneau, Framework for analytical quantification of disaster resilience, Eng. Struct. 32 (11) (2010) 3639–3649, https://doi.org/10.1016/j.engstruct.2010.08.008.

[21] M. Pregnolato, A. Ford, C. Robson, V. Glenis, S. Barr, R. Dawson, Assessing urban strategies for reducing the impacts of extreme weather on Infrastructure Networks, R. Soc. Open Sci. 3 (5) (2016) 160023, https://doi.org/10.1098/rsos.160023.

[22] A. Karduni, A. Kermanshah, S. Derrible, A protocol to convert spatial polyline data to network formats and applications to World Urban Road Networks, Sci. Data 3 (1) (2016), https://doi.org/10.1038/sdata.2016.46.

[23] P. Gauthier, A. Furno, N.-E. El Faouzi, Road network resilience: how to identify critical links subject to day-to-day disruptions, Transp. Res. Rec.: J. Transport. Res. Board 2672 (1) (2018) 54–65, https://doi.org/10.1177/0361198118792115.

[24] R.I. Ogie, T. Holderness, S. Dunn, E. Turpin, Assessing the vulnerability of hydrological infrastructure to flood damage in coastal cities of developing nations, Comput. Environ. Urban Syst. 68 (2018) 97–109, https://doi.org/10.1016/j.compenvurbsys.2017.11.004.

[25] A. Nelson, R. By, T. Thomas, S. Girgin, M. Brussel, V. Venus, R. Ohuru, The Resilience of Domestic Transport Networks in the Context of Food Security – a multi-country Analysis: Background Paper for the State of Food and Agriculture 2021, Food & Agriculture Org., 2021, p. 52, 2021.

[26] Y. Casali, H.R. Heinimann, A topological characterization of flooding impacts on the Zurich road network, PLoS One 14 (7) (2019) e0220338, https://doi.org/10.1371/journal.pone.0220338.

[27] Y. Alabbad, J. Mount, A.M. Campbell, I. Demir, Assessment of transportation system disruption and accessibility to critical amenities during flooding: iowa case study, Sci. Total Environ. 793 (2021) 148476, https://doi.org/10.1016/j.scitotenv.2021.148476.

[28] E. Henry, A. Furno, N. Faouzi, A Graph-based Approach with Simulated Traffic Dynamics for the Analysis of Transportation Resilience in Smart Cities, Presentation, Washington, D.C, 2021.

[29] S. Marshall, J. Gil, Street network studies: from networks to models and their representations, Network. Spatial Econ. 18 (3) (2018) 735–749, https://doi.org/10.1007/s11067-018-9427-9.

[30] J. Pung, R.M. D'Souza, D. Ghosal, M. Zhang, A road network simplification algorithm that preserves topological properties, Appl. Network Sci. 7 (1) (2022) 79, https://doi.org/10.1007/s41109-022-00521-8.

[31] J. Xia, F.Y. Teo, B. Lin, R.A. Falconer, Formula of incipient velocity for flooded vehicles, Nat. Hazards 58 (1) (2010) 1–14, https://doi.org/10.1007/s11069-010-9639-x.

[32] C. Shu, J. Xia, R.A. Falconer, B. Lin, Incipient velocity for partially submerged vehicles in floodwaters, J. Hydraul. Res. 49 (6) (2011) 709–717, https://doi.org/10.1080/00221686.2011.616318.

[33] F.Y. Teo, J. Xia, R.A. Falconer, B. Lin, Experimental studies on the interaction between vehicles and floodplain flows, Int. J. River Basin Manag. 10 (2) (2012) 149–160, https://doi.org/10.1080/15715124.2012.674040.

[34] M. Kramer, K. Terheiden, S. Wieprecht, Safety criteria for the trafficability of inundated roads in urban floodings, Int. J. Disaster Risk Reduct. 17 (2016) 77–84, https://doi.org/10.1016/j.ijdrr.2016.04.003.

[35] K.-S. Choo, D.-H. Kang, B.-S. Kim, Impact assessment of urban flood on traffic disruption using rainfall–depth–vehicle speed relationship, Water 12 (4) (2020) 926, https://doi.org/10.3390/w12040926.

[36] N. Wang, J. Hou, Y. Du, H. Jing, T. Wang, J. Xia, J. Gong, M. Huang, A dynamic, convenient and accurate method for assessing the flood risk of people and vehicle, Sci. Total Environ. 797 (2021) 149036, https://doi.org/10.1016/j.scitotenv.2021.149036.

[37] F. Shahdani, M. Santamaria-Ariza, H. Sousa, M. Coelho, J. Matos, Assessing flood indirect impacts on road transport networks applying mesoscopic traffic modelling: the case study of Santarém, Portugal, Appl. Sci. 12 (6) (2022) 3076, https://doi.org/10.3390/app12063076.

[38] P.D. Bates, A.P.J. De Roo, A simple raster-based model for flood inundation simulation, J. Hydrol. 236 (1-2) (2000) 54–77, https://doi.org/10.1016/s0022-1694(00)00278-x.

[39] M.S. Horritt, P.D. Bates, Evaluation of 1D and 2D numerical models for predicting river flood inundation, J. Hydrol. 268 (1-4) (2002) 87–99, https://doi.org/10.1016/s0022-1694(02)00121-x.

[40] I. Shustikova, A. Domeneghetti, J.C. Neal, P. Bates, A. Castellarin, Comparing 2D capabilities of HEC-RAS and LISFLOOD-FP on complex topography, Hydrol. Sci. J. 64 (14) (2019) 1769–1782, https://doi.org/10.1080/02626667.2019.1671982.

[41] P.D. Bates, J. Savage, O. Wing, N. Quinn, C. Sampson, J. Neal, A. Smith, A climate-conditioned catastrophe risk model for UK flooding, Nat. Hazards Earth Syst. Sci. 23 (2) (2023) 891–908, https://doi.org/10.5194/nhess-23-891-2023.

[42] R. De Risi, F. Jalayer, F. De Paola, I. Iervolino, M. Giugni, M.E. Topa, E. Mbuya, A. Kyessi, G. Manfredi, P. Gasparini, Flood risk assessment for informal settlements, Nat. Hazards 69 (1) (2013) 1003–1032, https://doi.org/10.1007/s11069-013-0749-0.

[43] K. He, N. Carhart, M. Pregnolato, J. Neal, R.D. Risi, Probabilistic Functionality Assessment of Road Networks for Medical Emergency Vehicles During Flooding, 2025. Manuscript submitted for publication.

[44] A.L.C. Bazzan, F. Klügl, A review on agent-based technology for traffic and transportation, Knowl. Eng. Rev. 29 (3) (2013) 375–403, https://doi.org/10.1017/s0269888913000118.

[45] M. Lu, S. Yan, Signal light optimization based on PTV Vissim software, IOP Conf. Ser. Mater. Sci. Eng. 688 (2019) 044003, https://doi.org/10.1088/1757-899x/688/4/044003.

[46] M.M. Fuertez, A.C.L. Aguinaldo, K.R. Cadungog, J.V.G. Lintag, J.B. Nicdao, J.I.M. Pangan, J.C. Villanueva, J.V.G. Tongol, J.M.B. Mandap, Traffic flow simulation using PTV Vissim: a proposed solution on Jose Abad Santos Avenue Road and Baliwag–Candaba–Sta. Ana Road intersection, Int. J. Progress. Res. Sci. Eng. 4 (6) (2023) 374–386.

[47] PTV Group, PTV Vissim: *traffic simulation software*, PTV Planung Transport Verkehr AG (2022). Retrieved from, https://www.ptvgroup.com/en/.

[48] D. Krajzewicz, J. Erdmann, M. Behrisch, L. Bieker, Recent development and applications of SUMO—Simulation of Urban MObility, Int. J. Agile Syst. Manag. 5 (3&4) (2012) 128–138.

[49] C. Zhuge, C. Shao, X. Yang, Agent- and activity-based large-scale simulation of enroute travel, enroute refuelling and parking behaviours in Beijing, China, J. Comput. Sci. 38 (2019) 101046.

[50] H. Triebke, M. Kromer, P. Vortisch, Bridging the gap between mesoscopic transport planning and microscopic traffic simulation: an analytical and numerical analysis of traffic dynamics, Transport. Res. Record J. Transport. Res. Board 2677 (5) (2022) 62–76, https://doi.org/10.1177/03611981221128284.

[51] S. Loreti, E. Ser-Giacomi, A. Zischg, M. Keiler, M. Barthélemy, Local impacts on road networks and access to critical locations during extreme floods, Sci. Rep. 12 (2022) 1552, https://doi.org/10.1038/s41598-022-04927-3.

[52] W. Wang, S. Yang, H.E. Stanley, J. Gao, Local floods induce large-scale abrupt failures of road networks, Nat. Commun. 10 (2019) 2114, https://doi.org/10.1038/s41467-019-10063-w.

[53] C. Zhuge, M. Bithell, C. Shao, X. Li, J. Gao, An improvement in MATSim computing time for large-scale travel behaviour microsimulation, Transportation (2019), https://doi.org/10.1007/s11116-019-10048-0.

[54] A. Jafari, D. Singh, A. Both, M. Abdollahyar, L. Gunn, S. Pemberton, B. Giles-Corti, Activity-based and agent-based transport model of Melbourne: an open multi-modal transport simulation model for Greater Melbourne, J. Intelligent Transport. Syst. (2024), https://doi.org/10.1080/15472450.2024.2372894. Advance online publication.

[55] B.Y. He, J. Zhou, Z. Ma, D. Wang, D. Sha, M. Lee, J.Y.J. Chow, K. Ozbay, A validated multi-agent simulation test bed to evaluate congestion pricing policies on population segments by time-of-day in New York City, Transp. Policy 101 (2021) 145–161, https://doi.org/10.1016/j.tranpol.2020.12.011.

[56] M. Maciejewski, J. Bischoff, Congestion effects of autonomous taxi fleets, Transport 33 (4) (2018) 971–980, https://doi.org/10.3846/16484142.2017.1347827.

[57] I. Kaddoura, K. Nagel, Congestion pricing in a real-world oriented agent-based simulation context, Res. Transport. Econ. 74 (2019) 40–51, https://doi.org/10.1016/j.retrec.2019.01.002.

[58] D. Ziemke, N. Kuehnel, C. Llorca, R. Moeckel, K. Nagel, FABILUT: the flexible agent-based integrated land use/transport model, J. Transport Land Use 15 (1) (2022) 497–526, https://doi.org/10.5198/jtlu.2022.2126.

[59] J.C. Herrera, D.B. Work, R. Herring, X.J. Ban, Q. Jacobson, A.M. Bayen, Evaluation of traffic data obtained via GPS-enabled mobile phones, Transport. Res. C Emerg. Technol. 18 (4) (2010) 568–583, https://doi.org/10.1016/j.trc.2009.10.006.

[60] J. Fan, C. Fu, K. Stewart, L. Zhang, Using big GPS trajectory data analytics for vehicle miles traveled estimation, Transport. Res. C Emerg. Technol. 103 (2019) 298–307, https://doi.org/10.1016/j.trc.2019.04.019.

[61] Y. Zhang, A. Loder, F. Rempe, K. Bogenberger, Temporal aggregated analysis of GPS trajectory data using two-fluid model, Transp. Res. Rec. 2677 (5) (2023) 103–116, https://doi.org/10.1177/03611981221128279.

[62] Md.S. Iqbal, C.F. Choudhury, P. Wang, M.C. González, Development of origin–destination matrices using mobile phone call data, Transport. Res. C Emerg. Technol. 40 (2014) 63–74, https://doi.org/10.1016/j.trc.2014.01.002.

[63] L. Alexander, S. Jiang, M. Murga, M.C. González, Origin–destination trips by purpose and time of day inferred from mobile phone data, Transport. Res. C Emerg. Technol. 58 (2015) 240–250, https://doi.org/10.1016/j.trc.2015.02.018.

[64] J.L. Toole, S. Colak, B. Sturt, L.P. Alexander, A. Evsukoff, M.C. González, The path most traveled: travel demand estimation using big data resources, Transport. Res. C Emerg. Technol. 58 (2015) 162–177, https://doi.org/10.1016/j.trc.2015.04.022.

[65] I.H. Naser, M.B. Mahdi, F.H. Meqtoof, H.A. Etih, Modelling trip distribution using the gravity model and Fratar's method, Math. Model. Eng. Problems 8 (2) (2021) 230–236, https://doi.org/10.18280/mmep.080209.

[66] G. Boeing, OSMnx: new methods for acquiring, constructing, analyzing, and visualizing complex street networks, Comput. Environ. Urban Syst. 65 (2017) 126–139, https://doi.org/10.1016/j.compenvurbsys.2017.05.004.

[67] Bristol City Council, *Bristol Census 2021 dashboard* [PDF]. https://www.bristol.gov.uk/files/documents/6297-bristol-census-dashboard, 2023.

[68] M. Lenormand, A. Bassolas, J.J. Ramasco, Systematic comparison of trip distribution laws and models, J. Transport Geogr. 51 (2016) 158–169.

[69] N. Geroliminis, C.F. Daganzo, Existence of urban-scale macroscopic fundamental diagrams: some experimental findings, Transp. Res. Part B Methodol. 42 (9) (2008) 759–770.

[70] J. Pereira, A. Pasquali, P. Saleiro, R. Rossetti, Transportation in social media: an automatic classifier for travel-related tweets, Lect. Notes Comput. Sci. (2017) 355–366, https://doi.org/10.1007/978-3-319-65340-2_30.

[71] Kamil Raczycki, Marcin Szymański, Yahor Yeliseyenka, Piotr Szymański, Tomasz Kajdanowicz, Spatial data mining of public transport incidents reported in social media, ArXiv (Cornell University) (2021) 1–8, https://doi.org/10.1145/3486629.3490696.

[72] Y. Liao, S. Yeh, J. Gil, Feasibility of estimating travel demand using geolocations of social media data, Transportation 49 (1) (2021) 137–161, https://doi.org/10.1007/s11116-021-10171-x.

[73] A. Sevtsuk, R. Kalvo, Patronage of urban commercial clusters: a network-based extension of the Huff model for balancing location and size, Environ. Plan. B Urban Anal. City Sci. 45 (3) (2017) 508–528, https://doi.org/10.1177/2399808317721930.

[74] J. Gil, Street network analysis "edge effects": examining the sensitivity of centrality measures to boundary conditions, Environ. Plan. B Urban Anal. City Sci. 44 (5) (2016) 819–836, https://doi.org/10.1177/0265813516650678.

[75] Office for National Statistics, *Car or van availability, Census 2021* (Table TS045). https://www.ons.gov.uk/datasets/TS045/editions/2021, 2023.

[76] Barratt Developments, *Average house sizes UK*. David Wilson Homes, from, https://www.dwh.co.uk/advice-and-inspiration/average-house-sizes-uk/, 2024. (Accessed 22 February 2025).

[77] Office for National Statistics, Admin-based statistics for property floor space: feasibility research, England and Wales. https://www.ons.gov.uk/peoplepopulationandcommunity/housing/methodologies/adminbasedstatisticsforpropertyfloorspacefeasibilityresearchenglandandwales, 2022.

[78] University of Colorado Boulder, Campus Planning Study: Space Allocation Guidelines. Boulder, CO, University of Colorado Boulder, 2021.
[79] The Engineering ToolBox (2003). *Required Room Space per Person*. [online] Available at: https://www.engineeringtoolbox.com/number-persons-buildings-d_118.html [Accessed 30 August 2025].
[80] W. Yu, M. Guan, Z. Chen, Analyzing spatial community pattern of network traffic flow and its variations across time based on taxi GPS trajectories, Appl. Sci. 9 (10) (2019) 2054, https://doi.org/10.3390/app9102054, 2054.
[81] MATSim User Guide, MATSim user guide, Retrieved from, Version 0.6.0, 2014. https://svn.vsp.tu-berlin.de/repos/public-svn/publications/vspwp/2014/14-20/user-guide-0.6.0-2014-09-12.pdf.
[82] D. Coles, D. Yu, R.L. Wilby, D. Green, Z. Herring, Beyond 'flood hotspots': modelling emergency service accessibility during flooding in York, UK, J. Hydrol. 546 (2017) 419–436, https://doi.org/10.1016/j.jhydrol.2016.12.013.
[83] D. Green, D. Yu, I. Pattison, R. Wilby, L. Bosher, R. Patel, P. Thompson, K. Trowell, J. Draycon, M. Halse, L. Yang, T. Ryley, City-scale accessibility of emergency responders operating during flood events, Nat. Hazards Earth Syst. Sci. 17 (1) (2017) 1–16, https://doi.org/10.5194/nhess-17-1-2017.
[84] CHANGE, The new ambulance standards [PDF], 1-5). Retrieved 29 May 2025, from, https://www.england.nhs.uk/wp-content/uploads/2017/07/new-ambulance-standards-easy-read.pdf, 2022.
[85] A. Horni, K. Nagel, K.W. Axhausen (Eds.), The multi-agent transport simulation MATSim, Ubiquity Press, 2016. https://doi.org/10.5334/baw.
[86] K.W. Axhausen, The application of multi-agent simulation models in transportation: methods, models, and case studies, Transp. Rev. 33 (6) (2013) 647–665, https://doi.org/10.1080/01441647.2013.770631.
[87] Transportation Research Board, *Highway Capacity Manual* (Special Report 209), National Research Council, Washington, DC, 2000.